Sandia National Laboratories

Operated for the United States Department of Energy
by National Technology and Engineering Solutions
of Sandia, LLC.
Albuquerque, New Mexico 87185-0747
Livermore, California 94551-0969

date: 9 March 2026

STEPHEN WAGNER (Affiliate) Digitally signed by STEPHEN WAGNER (Affiliate) Date: 2026.03.09 12:35:02 -06'00'

to: Steve Wagner, 8881
Ross Kirkes, 8881

from: Rob P. Rechard, 8844
Patrick V Brady, 8800

subject: Hydrologic and Geochemical Constraints on Post-Closure Criticality in Geologic Media Near Waste Isolation Pilot Plant

ABSTRACT

This report describes the hydrologic and geochemical constraints that prevent assembling a critical mass of fissile mass after closure of the Waste Isolation Pilot Plant (WIPP), an operating geologic repository in southeastern New Mexico for the disposal of transuranic (TRU) waste from atomic energy defense activities. For most TRU waste, concern about post-closure criticality has been low because of the low mass and low concentration of fissile material (mostly plutonium) in containers, the low concentrations of fissile material released because of sorption and low solubility, and the natural tendency of fissile solute to disperse during transport. However, the disposal of TRU wastes in containers with more mass and higher concentrations of fissile material prompted an updated evaluation of the criticality potential. Molecular diffusion limits forming micro-environments favorable to fissile deposition in the repository. The uniform distribution of iron (from the containers) and magnesium oxide (added in the disposal area) keeps the brine chemistry fairly uniform such that pH, ionic strength, and reduction-oxidation potential do not vary widely, on a macroscopic scale, and thereby cause fissile deposition in preferential regions of the repository. Hydrologic constraints limit most fissile deposition to the Culebra dolomite strata above the repository after a hypothetical inadvertent intrusion into WIPP. The typically low solubility of plutonium and uranium implies that vast amounts of brine are required to transport enough fissile material to the Culebra dolomite to cause criticality. The large amount and variability of the brine flux spreads out the mixing zone if precipitation were to occur through changes in ionic strength and pH. The large mixing zone is such that the plutonium and uranium concentration remain below criticality limits. Although sorption occurs throughout the WIPP disposal system, it is not sufficient to assemble a critical concentration. Finally, thermodynamic equilibrium of dissolved plutonium with any colloidal plutonium in a destabilization/filtration region of the WIPP disposal system limits the ability of colloids to exceed the solution concentration by orders of magnitude.

Keywords: post-closure criticality evaluation; feature, event, and process screening; transuranic radioactive waste disposal; safety assessment; performance assessment; Waste Isolation Pilot Plant

Information Only

FOREWARD

The nuclear criticality evaluations and calculations referenced within this document are published to meet the requirements of the US Environmental Protection Agency's (EPA) implementing regulation, 40 CFR §194.32(e)(3). The nuclear criticality evaluations and calculations are relied on to justify the exclusion of nuclear criticality impacting the Waste Isolation Pilot Plant (WIPP) disposal system during the post-closure regulatory timeframe. This justification is performed in accordance with EPA "reasonable expectation" standard of proof given in 40 CFR §191.13(b) for the post-closure timeframe. This report is being issued outside of Sandia National Laboratories' Nuclear Criticality Safety Program that is governed under 10 CFR 830 and US Department of Energy (DOE) Order 420.1C, Chg. 3 without receiving that program's concurrence or dissension of the conclusions made within.

PREFACE

EPA has regulatory authority for certifying the performance of WIPP in isolating transuranic radionuclides over the next 10 000 years against its long-term environmental standard specified in 40 CFR 191. DOE, who is responsible for WIPP, has assigned Sandia National Laboratories (Sandia) to evaluate WIPP post-closure performance for EPA certification. Part of the performance assessment includes a formal analysis of all features, events, and processes (FEPs) that may impact WIPP isolation.

EPA does not designate the post-closure criticality FEP for special consideration in 40 CFR 191. Rather, criticality is considered like all other FEPs. The EPA Standard, 40 CFR 191, is probabilistic and Sandia has developed a probabilistic rationale that criticality is improbable in the post-closure timeframe when humans are absent, using EPA exclusion criteria specified in its implementing regulation, 40 CFR 194, at §194.32(e)(3). Specifically, this report evaluates the small fissile masses and concentration possible in the geologic setting in and around WIPP. The evaluation results are then compared to rough estimates of the large fissile masses and concentration necessary for criticality in a geologic setting to show that criticality is improbable during the 10 000-year period after WIPP closure.

In 40 CFR 194, EPA requires compliance evaluations for WIPP about every 5 years. Thus, the screening rationale for omitting the post-closure criticality FEP is periodically documented in certification applications to EPA, along with the compliance evaluation. The first application to EPA was in 1996. The most recent Compliance Recertification Application was in 2019. This report supports the 2026 Compliance Recertification Application.

We refer to the analysis underlying the rationale as a post-closure criticality evaluation. Estimates of mean criticality behavior are used for this post-closure criticality evaluation, not worst-case behavior, in keeping with the concept of reasonable expectation invoked by EPA as the standard of proof for demonstrating compliance with 40 CFR 191. We avoid referring to the criticality screening as a credibility argument because the term connotes a rule-based approach that estimates worst-case behavior and uses great care in conservatively defining an upper subcriticality limit.

This report updates the 2019 memorandum by R.P. Rechard and E.R. Stein, *Hydrologic and Geochemical Constraints on Criticality in Geologic Media near Bedded Salt Repository*, which supported the 2019 WIPP Compliance Recertification Application to EPA.

ACKNOWLEDGEMENTS

Tara LaForce and Mariah Garcia of Sandia National Laboratories and G. Ross Kirkes of Piru Associates conducted the internal technical review.

Information Only

Contents

I. Introduction 9
I.A. Regulatory Guidance for Screening Criticality 9
I.B. Criticality Scenario Subsets Considered in Low-Probability Rationale 11
I.C. Human Disruption 11
I.D. Approximation of Mean Probability of Criticality 12
II. WIPP Disposal System 12
II.A. Transuranic Waste 12
II.A.1. General Categories of TRU Waste. 12
II.A.2. Surplus Plutonium 12
II.A.3. TRU Containers 13
II.B. Geologic Characteristics of WIPP Disposal System 14
II.B.1. Castile Formation 14
II.B.2. Salado Formation 14
II.B.3. Culebra Dolomite Member of Rustler Formation 15
II.C. Repository Design 15
III. Neutronic constraints 16
III.A. Critical Mass and Concentration in Mixtures of Brine and Geologic Media 16
III.B. Geometric Constraints on Deposition in Anhydrite Layers and Boreholes near Repository 18
III.C. Regulatory Constraint at Disposal System Boundary 18
IV. Dissolved Fissile Concentration 18
IV.A. Solubility Model and Oxidation State Analogy 18
IV.B. Oxidation State Dependence 19
IV.C. Brine Dependence 19
IV.D. Brine Mixing Volume 19
IV.E. Organic Ligand Concentration 19
IV.F. pH Dependence and MgO Control 19
IV.G. Actinide Solubility at Minimum Brine Mixing Volume 20
IV.H. Uncertainty in Solubility. 20
IV.I. Comparison of Criticality Limits to Dissolved Concentration 21
V. Colloidal Fraction 21
V.A.General Fate of Colloids in Rooms prior to Intrusion 21
V.B. General Constraint on Colloidal Filtration in Repository after Intrusion 22
V.C.Colloidal Fraction of Total Fissile Concentration 22
V.D. Concentration of Colloids 25
VI. Sorption Of Fissile Material 25
VI.A. General Constraints on Sorption in Repository 26
VI.B. Macroscopic Scale in Repository 26
VI.C. Sorption Process 26
VI.D. Geochemical Constraint on Sorption in Repository 27
VI.E. Constraint on Sorption in Culebra Dolomite 27
VII. Precipitation 28
VII.A. Constraint on Precipitation in Disposal Area 28
VII.B. Constraints on Precipitation in Culebra: Lack of Favorable Depositional Features 28
VIII. Hydrologic Constraints From PA Modeling 29
VIII.A. Modeling Scenarios 29
VIII.B. Hydrologic Constraint on Brine Movement Prior to Inadvertent Intrusion 30
VIII.C. Hydrologic constraints on Deposition in Culebra Dolomite after Inadvertent Intrusion 31
IX. Geochemical Constraints in Culebra from PA Modeling 31
IX.A. Fissile Release to Culebra 31
IX.B. Supplemental Analysis of Pu Dispersion in Culebra 33
IX.C. Lack of Conditions for Precipitation in Culebra 36

Information Only

IX.D. Lack of Conditions for Sorption in Culebra....37
X. Summary: Rationale for Hydrologic and Geochemical Constraints on Criticality in WIPP Disposal System ..38
X.A. Constraints within Repository Prior to Hypothetical Human Disruption....38
X.B. Constraints within Repository After Hypothetical Human Disruption....38
X.C. Constraints in Culebra After Hypothetical Human Disruption....38
References 42

Information Only

FIGURES

1. WIPP repository 42 km east of Carlsbad, located in Delaware Basin of Permian Basin in southeastern New Mexico.[2, Fig. 1] 9
2. Pathways to criticality at WIPP including geomechanical compaction, hydrologic movement, and geochemical mobilization/deposition in underground facility and geologic barrier before and after human intrusion. 11
3. Stratigraphy above and below the WIPP repository with elevation contacts referenced to ERDA-9.[2, Fig. 4;52] 14
4. Idealized model stratigraphy around WIPP disposal rooms in lower horizon (rooms in Panels 1, 2, 7, 8, and 10); and rooms in upper horizon (Panels 3, 4, 5, and 6) with elevations referenced to Clay G seam, which is at elevation 386 m, 652 m below surface at exploratory well ERDA-9.[52;53, Fig. 1] 15
5. Transuranic waste disposal area of the WIPP repository has 8 panels and one equivalent panel in the north central region; EPA has authorized 2 replacement panels to the west;[15] 7 additional panels have also been proposed to the west.[14] 16
6. Critical mass and concentration limits for homogeneous spherical shape of Pu in various materials at 20% porosity saturated with WIPP brines.[26, Fig. 35;28, Fig. 28] 16
7. Criticality limits for 5% enriched ^{235}U deposited in homogeneous spherical shape in various material at 20% total porosity saturated with WIPP brines.[26, Figs. 34&36;27, Fig. 6;28] 17
8. Critical radius for PuO_2 and UO_2 in various media with 20% porosity filled with water and WIPP brines data.[26, Figs. 37&38;28]) 17
9. Homogeneous system of ^{239}Pu and ^{235}U is always more reactive than heterogeneous system for fracture spacing occurring in Culebra dolomite.[26, Fig. 29;28, Fig. 26] 18
10. Mean, median, and range of actinide dissolved solution concentration (without colloids) for 3+, 4+, and 6+ oxidation states in disposal rooms at minimum brine mixing volume for WIPP certifications. 21
11. Hypothetical future release of radionuclides to the Culebra after disruptive human intrusion into repository in Scenario A_{E2E1}.[2, Fig. 2;31, Figure 5.1-2] 29
12. Distribution of individual ^{239}Pu and ^{235}U cumulative releases to Culebra for computational scenario A_{E2E1}-BF-t100 when all 3 replicates combined for CRA-26-19P, CRA-26-12P, RPPCR-23-19P, and CRA-2019. 31
13. Cumulative volume and flow rate of brine and cumulative Pu mass and flux into Culebra over 10,000 years from an intrusion that occurs 100 years after closure in Replicate 2 of CRA-2019 (A_{E1}-BF-t100-r2). 32
14. Plume of non-adsorbing tracer in Culebra at intrusion borehole between 310 years and 2000 years with brine flux of 72 000 m^3 in run 68 of computational scenario A_{E1}-BF-t100-r2; lines at borehole are 5 m, 10 m, and 15 m long; boxes are 50 m and 100 m on a side; contours are at normalized tracer release of 0.001, 0.2, 0.4, 0.6, and 0.8. 34
15. Plume of non-adsorbing tracer in Culebra at intrusion borehole between 310 years (10 years after plug to Castile brine source fails in 100-year intrusion) and 2000 years (800 years after salt creep closes off Castile brine source) with mean brine flux of all 100 runs of scenario A_{E1}-BF-t100-r2. 35
16. Average Darcy velocity between 10.5 and 9.0 m/s, standard deviation between 0 and 0.6 m/s, and directional standard deviation between 0 and 0.3 of $\tan^{-1}(v_y/v_x)$ above WIPP panels (small black rectangle) for 300 flow fields of scenario where potash mining disrupts the Culebra flow field. The large rectangle is the land withdrawal boundary.[106, Figure 4-3] 36

Information Only

TABLES

I. Projected fissile material at WIPP closure for selected certifications. 13
II. Average iron mass emplaced in high-count payload containers by 31 December 2021.[50, Table 4] 13
III. Mass of major components of TRU waste in recent performance assessments. 14
IV. Minerals in Culebra Dolomite strata.[26, Table II;28, Table II;54, p. 3-9] 15
V. MgO mass and volume emplaced in WIPP Rooms 15
VI. Composition of Culebra, Salado, and Castile brines near WIPP. 17
VII. Example of Mean and Maximum Total Plutonium and Uranium Concentration in Castile Brine from Dissolved and Four Colloidal Types for CRA-2019 and CRA-2026. 25
VIII. Sorbent mass, surface area, and sorption coefficients for iron corrosion products and hydrated magnesium oxide 26
IX. Designation of Computational Scenarios for Modeling Brine Flow and Repository Radionuclide Transport from Intrusion into the WIPP Repository.[100, Table 5] 30
X. Mean cumulative brine flow out of repository and up intrusion borehole in CRA-2019.[101, Table 23] 30
XI. Mean and maximum cumulative brine and Pu releases to Culebra in A_{E1}-BF-t100 of CRA-2019 32
XII. Mixing zone and corresponding Pu concentration for E1 intrusion at 100 years and Castile plug failure 200 years later in CRA-2019 (Scenario A_{E1}-BF-t100-r2) 37
XIII. Rationale for Low Probability of Criticality from hydrologic and geochemistry processes in WIPP Disposal System 40

Information Only

ACRONYMS AND INITIALISMS

CCA	compliance certification application (to EPA)
CCDF	complementary cumulative distribution function (performance measure in EPA disposal standard at Title 40 Code of Federal Regulations Part 191)
CCO	criticality control overpack (container)
CH-TRU	contact handled transuranic (waste)
CFR	Code of Federal Regulations
CRA	compliance re-certification application (to EPA)
DOE	US Department of Energy
DRZ	disturbed rock zone
E1	inadvertent intrusion into repository and pressurized brine source in Castile Fm scenario class
E2	inadvertent intrusion into repository scenario class
E2E1	combination of E2 and E1 scenario classes
EDTA	ethylenediaminetetraacetate
EPA	US Environmental Protection Agency
EQ3/6	software package for geochemical modeling of aqueous systems
FEP	features, events (natural and anthropogenic phenomena of short duration), and processes (natural phenomena of long duration)
FME	fissile mass equivalent
PA	performance assessment is process of assessing whether a system or component meets a set of performance criteria. For US, the process is a stochastic simulation; the system is a deep geologic repository disposal system; the performance criteria are the long-term measures in the EPA post-closure environmental standard 40 CFR 191
PAVT	PA verification test (for EPA)
PFLOTRAN	software package for modeling subsurface flow and transport
POC	pipe overpack container
RH-TRU	remote handled transuranic (waste)
RPPCR	replacement panel planned change request (to EPA)
TRU	transuranic (radioactive waste)
TRUPACT-II	Transuranic Package Transporter Model 2
US	United States
WIPP	Waste Isolation Pilot Plant (repository in southeastern New Mexico for TRU waste from atomic energy defense activities)

Information Only

Information Only

I. INTRODUCTION

As with other nuclear facilities, the possibility of sufficient fissile mass and concentration causing a self-sustained neutron chain reaction (here after termed criticality) must be evaluated for geologic disposal systems.[1] This paper discusses the potential of criticality sometime in the future after closure of the Waste Isolation Pilot Plant (WIPP), a repository in 600-m thick bedded salt in southeastern New Mexico for the geologic disposal of wastes containing transuranic (TRU) radioisotopes from atomic energy defense activities (Fig. 1).

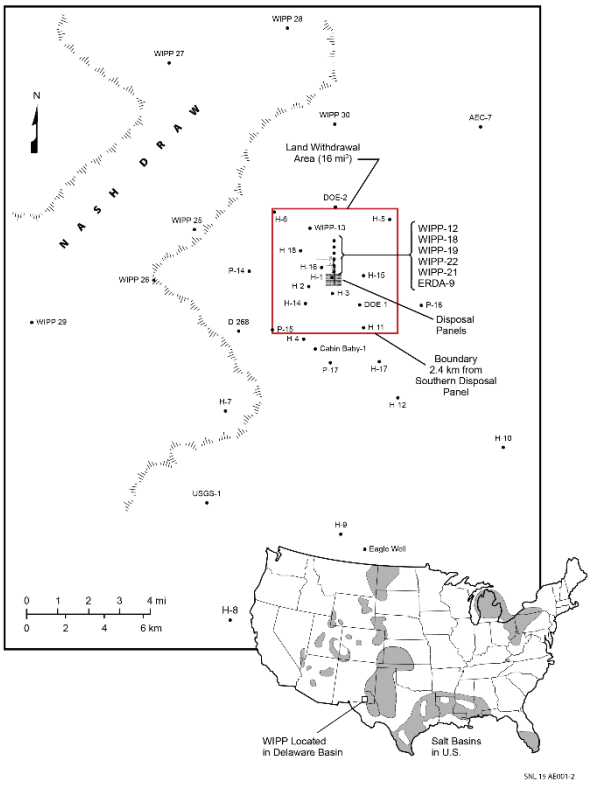

Fig. 1. WIPP repository 42 km east of Carlsbad, located in Delaware Basin of Permian Basin in southeastern New Mexico.[2, Fig. 1]

In the *WIPP Land Withdrawal Act of 1992* Congress designated EPA as the regulator of WIPP.[3] In response, EPA promulgated criteria in Title 40 Code of Federal Regulations Part 194 (40 CFR 194)[4;5] on how the US Department of Energy (DOE) was to show compliance with its radiation protection standard for nuclear waste disposal in 40 CFR 191[6;7] In 40 CFR 194, EPA requires that DOE (operator of WIPP) document continued compliance about every 5 years, which implies periodic review of all features, events, and processes (FEPs) included or excluded from a compliance evaluation.[8] Hence, a renewed evaluation has been undertaken of the likelihood of assembling a critical mass from fissile material in TRU waste disposed after WIPP closure (i.e., post-closure criticality).

In the past, concern about post-closure criticality has been low because of the low concentration of fissile material in TRU waste, small concentrations of fissile material released because of sorption and low solubility, and the natural tendency of fissile solute to disperse during transport, as discussed in the Compliance Certification Application in October 1996[5;9;10] and summarized in 2001 and 2015.[1;2;11] However, the criticality evaluation has been expanded because pipe overpack containers (POCs) and criticality container overpacks (CCOs) destined for WIPP may have higher fissile content than containers examined in 1996.[12]

The information and results presented here consider inventory, repository design, and analysis modeling changes related to post-closure criticality for the most recent 2019 Compliance Re-certification Application (CRA-2019)[13] and the current 2026 Compliance Re-certification Application, which is the fifth re-certification application submitted to EPA (CRA-2026). CRA-2019 disposed 10.3 t Pu surplus to defense needs. In addition, a change request to add 2 replacement panels with a portion of 7.1 t additional surplus Pu was submitted in 2023 and approved by EPA (replacement panel planned change request—RPPCR-23).[14;15]

In CRA-2026, an additional 26.9-t surplus Pu waste is considered.[16;17] The total surplus Pu will eventually be considered in a supplemental environmental impact statement to add seven additional panels to the WIPP repository to accommodate the surplus Pu.

Two performance assessments (PAs)/sensitivity analyses were performed for both RPPCR-23 and CRA-2026: (1) PA for an interim repository layout consisting of 12 panels (designated RPPCR-23-12P[18] and CRA-26-12P), and (2) PA for final repository layout consisting of 19 panels (designated RPPCR-23-19P[14] and CRA-26-19P when it is necessary to be specific).

I.A. Regulatory Guidance for Screening Criticality

EPA does not provide separate guidance regarding the occurrence of post-closure criticality in either 40 CFR 191 or 40 CFR 194.[4-7] Rather, criticality is evaluated within the probabilistic regulatory framework for disposal and considered along with other FEPs and scenario classes of the disposal system.

In Appendix C of 40 CFR 191[6;7] and in 40 CFR 194.32,[4;5] EPA provides three criteria for excluding FEPs or scenario classes,[a] such as criticality, from the PA

[a] Within the WIPP Project, a scenario is a set of FEPs that outlines a possible future condition but does not include the timing or ordering of events and processes. Once a mathematical model of the disposal system is developed, timing and order of events and processes are

Information Only

over the 10^4-year regulatory period: (1) regulatory fiat (e.g., EPA guidance excluding changes in society or technology for inadvertent human intrusion); (2) low consequence to magnitude of expected radionuclide release, and (3) low probability of occurrence. Exclusion of low probability FEPs is via (a) a quantitative demonstration that the probability is $<10^{-4}$ over 10^4 years (e.g., probability of massive meteor strike disrupting WIPP repository 658 m underground), (b) qualitative argument that the FEPs and scenario classes are improbable based on site, waste, or repository characteristics (e.g., lack of credible occurrence of tsunami event in the interior of the North American continent); or (c) reasoned qualitative rationale that argues against the likelihood of a FEP occurring.[6,Appendix B;7, Appendix C] Certainly approaches (b) and (c) are closely related, and often not separately identified. The approaches are separated here since the effort expended on the reasoned qualitative rationale omitting the criticality FEP has been extensive. This report updates this qualitative low-probability rationale to exclude criticality in the underground facility and in formations above the underground facility.

A subtle question is whether the basis of low probability (or low consequence) should use analysis completely separate from the PA analysis and demonstrate exclusion of, for example, the criticality FEP without information from PA iterations or whether an equally valid approach is where one makes an hypothesis that a FEP can be screened out, conducts the PA, and then verifies that the hypothesis of exclusion is correct by using the specifics of the PA results (e.g., concentrations of fissile material in the repository or overlying Culebra dolomite strata).[20, §2.1] When we speak of using results separate from the PA, we mean an analysis that does not depend on either intermediate or final PA results. We wish to emphasize that use of results from the last iteration of a PA, rather than the current PA, does not provide separation from the PA analysis. Though conducted at different times, the previous PAs are not separate from the current PA since the current PA builds upon previous PAs. The current PA involves the best current understanding of the WIPP disposal system and the previous PA may not properly reflect this updated understanding.

A conceptual advantage of using analysis separate from the PA analysis is that the rationale for excluding a FEP may appear less ephemeral since the rationale is not tied to a particular PA iteration. Furthermore, this approach avoids the question of whether the PA analysis is conducted at the proper scale to screen the FEP.

However, the separation of a FEP rationale from the PA is somewhat illusionary especially as regards low consequence reasoning. The significance of an estimate of the cumulative release with or without a FEP and, thereby, the consequence screening rationale must recognize the current PA estimate of cumulative release to determine significance if the estimate of cumulative release including the FEP is anything but trivially small. Because this relative comparison with and without a FEP is an important aspect of screening, it is not unexpected that a phenomenon that was screened out in an earlier PA iteration would be screened in for later PA iterations. Knowledge in a current PA iteration may improve about a process dominating radionuclide release in an earlier PA iteration, which results in its reduction such that other previously excluded FEPs now contribute a higher percentage to the summed cumulative release. For example, the importance of radiolysis of brine at WIPP was initially excluded because of its minor importance relative to other processes but is now included because the process now provides a somewhat larger contribution to the summed release.

Criticality represents a FEP for which an analysis completely separate from the PA is difficult: the criticality probability and consequence cannot be cleanly separated.[b] Criticality consequences are a strong function of the initial and boundary conditions under which a nuclear reaction would occur. In turn, the initial and boundary conditions of the fissile configuration analyzed must have a reasonable probability of occurring. It is the PA analysis that provides the information on the reasonable possibility of a fissile configuration occurring.

In this paper, modeling of geophysical processes conducted for the PAs underlying CRA-2019 and CRA-2026 supports the qualitative discussion on the absence of favorable hydrologic and geochemical processes (mobilization, transport, precipitation, sorption, and colloid aggregation) that could assemble fissile ^{239}Pu and ^{235}U radionuclides and lead to a critical mass/concentration. For the most part, intermediate results of CRA-2019[13] and CRA-2026 are used here to form the rationale but a few supplemental analyses, based on the models of CRA-2019, are also used.

As an example, fissile releases to the overlying Culebra dolomite are used to determine if (1) enough fissile material is present for criticality to occur in a geologic setting, and (2) whether the manner of release is such that it promotes forming a criticality assembly. Whether or not the criticality occurs in the overlying Culebra dolomite strata does not influence whether the

introduced. As used here, a scenario class is "a set of related scenarios sharing sufficient similarities that they can be aggregated for the purpose of screening analysis…"[19] and PA modeling. No sharp distinction exists between scenario and scenario class rather a continuum exists.

[b] Thus, the risk combination of probability and consequence of the criticality FEP provides an useful viewpoint that is discussed in a companion report.[21]

Information Only

fissile material is released to the Culebra dolomite strata and, thus, are separate phenomena.

I.B. Criticality Scenario Subsets Considered in Low-Probability Rationale

We discuss the low probability rationale for criticality at WIPP as the sum of probabilities from *m* computational scenarios ($\mathcal{A}_m^{CS}$) (or scenario subsets) to conceptually organize the various arguments in the rationale.

Two companion reports discuss the geomechanical process of disposal room closure, through salt creep, compacting TRU waste containers along with nuclear criticality modeling pertinent to assemblies of compacted containers. [22-25] These two reports consider the container type feature such as contact-handled TRU (CH-TRU) drums/boxes, remotely handled TRU (RH-TRU) canisters, POC packages, and CCO packages (Fig. 2). However, container types are only important in the disposal room prior to extensive degradation of the WIPP containers because Pu release to the geologic barrier is controlled by sorption or solubility (as discussed in §V). A third companion report summarizes the low probability and low consequence of criticality.[21]

This paper focuses on hydrologic constraints on fissile mobilization, and geochemical constraints on precipitation, sorption, and colloidal aggregation/filtering that prevent criticality in the underground facility and natural geologic barrier system. Features considered include locations such as the disposal rooms, elsewhere in the disposal area of the repository, and the Culebra dolomite strata above the repository in the geologic barrier (Fig. 2). Other locations considered in the 1996 CCA include the disturbed rock zone around the repository, anhydrite marker beds in the Salado, and the small diameter abandoned exploratory borehole. However, these locations are not numerated here since the amount of contaminated brine inflow (and subsequent fissile deposition) is bounded by fluid flow in the repository and into the Culebra dolomite.[1,§3.5;2, §IV.B]

The discussion herein is supported by a report on neutronic criteria (i.e., fissile type, mass, concentration, shape, spacing, mixed material, and nearby material) necessary for criticality after fissile deposition in geologic media (Fig. 2).[26-28] In combination, these papers support eliminating criticality events from consideration in WIPP performance assessments.

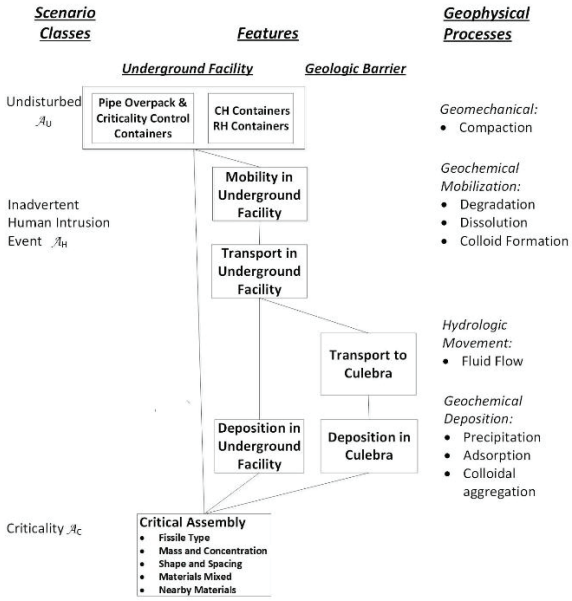

Fig. 2. Pathways to criticality at WIPP including geomechanical compaction, hydrologic movement, and geochemical mobilization/deposition in underground facility and geologic barrier before and after human intrusion.

I.C. Human Disruption

In 40 CFR 191 and 40 CFR 194,[6;7;29] EPA requires DOE demonstrate that the closed WIPP repository will comply with the performance criteria after hypothetical human disruption of the WIPP disposal system. However, EPA narrowed the focus of regulatory interest of human disruptions to[4;7] (a) fluid injection boreholes for deep oil reservoir recovery (that cause fluid injection into repository), (b) development of existing and future oil and gas wells (that cause seepage and subsidence), c) potash mining in the McNutt Potash Zone (that causes subsidence in Culebra dolomite and thereby influences flow); and (d) inadvertent intrusion into the repository via an exploratory borehole using present drilling technology.[30]Consideration of existing and future oil and gas wells and fluid injection into the repository (items a and b) are FEPs excluded from consideration in the WIPP PA.[13, App. SCR] Potash mining and exploratory borehole intrusion (items c and d) are included FEPs.

Without exploratory borehole intrusion to disrupt and allow brine to pass through the repository, there is no large driving force for the movement of radioisotopes (beyond diffusion through the salt). Hence, the exploratory borehole intrusion scenario is fundamental to the advective movement and assembly of fissile material beyond the disposal room, as demonstrated in the first PA in 1989 and thereafter.[5;31-33]Other FEPs particularly processes, that may disrupt the WIPP disposal system are considered during FEP screening (e.g., Ref[13, App. SCR-2019]).

Information Only

The short-term result of borehole intrusion is entrainment of wastes into the drilling fluid and their immediate release at the surface. Drilling debris with radionuclides at the surface already represents a release from the disposal system to the accessible environment, and so the potential for criticality in the drilling debris is not necessary to consider. Rather, it is the possibility of enhanced releases caused by criticality inside the disposal system that is explored here.

Sometime after intrusion, fissile material may move to other parts of the underground facility or up through the abandoned borehole, as discussed further in §VIII.A. In the EPA defined stylized calculation, the borehole, filled with material that has the permeability of silty sand, creates an advective path from the WIPP disposal rooms to the overlying Culebra dolomite strata but retains the remainder of the Culebra dolomite natural barrier, where transport of fissile material is likely dispersed.

I.D. Approximation of Mean Probability of Criticality

Consistent with the use of reasonable expectation and mean results in a PA,[34, §191.13 (b)] EPA guidance implies a mean estimate of a FEP or scenario class probability, such as criticality, provides an adequate estimate for screening. Consequently, EPA does not expect nor does the WIPP Project provide worse-case scenarios that combine unrealistic combinations of imagined events to assemble fissile material in order to discuss criticality after WIPP closure.

II. WIPP DISPOSAL SYSTEM

The likelihood of assembling a critical mass in or near a repository after closure depends upon (1) the type, form, and initial masses of fissile material; (2) the location and type of host geology, which determine the hydrologic and geochemical process present in the disposal system; and (3) the ability of the hydrologic and geochemical processes to concentrate enough fissile mass to meet the criteria necessary for a criticality scenario. The first two aspects are discussed here, the remainder of the paper discusses the third aspect.

II.A. Transuranic Waste

II.A.1. General Categories of TRU Waste.

As defined by EPA, material contaminated with α-emitting TRU radionuclides with an activity > 3.7 MBq/kg (>100 nCi/g) and half-life of >20 years requires deep geologic disposal.

As specified in the *Waste Isolation Pilot Plant Land Withdrawal Act*, WIPP disposes of two categories of TRU waste generated from atomic energy defense activities:[3;5] (1) CH-TRU, and (2) RH-TRU. TRU waste disposed in the past at WIPP has consisted of a variety of organics, inorganics, and solidified materials contaminated with TRU radionuclides.

The projected CH-TRU average ^{239}Pu enrichment of 90% for CRA-2019 and 92% for CRA-2026 are similar to the 90% ^{239}Pu enrichment projected for the 1996 CCA. The projected RH-TRU average ^{239}Pu enrichment at emplacement of 78% for CRA-2019 and 73% for CRA-26-19P has decreased from 88% projected for the 1996 CCA (Table I).

The projected ^{235}U enrichment of CH-TRU at emplacement is 1.8% for CRA-2019 and 0.26% for CRA-26-19P and has remained less than the 4.9% projected in the 1996 CCA. The RH-TRU ^{235}U enrichment of 8.4% for CRA-2019 and CRA-26-19P at WIPP closure are similar to the 6.5% enrichment projected in the 1996 CCA (Table I).

II.A.2. Surplus Plutonium

Since 1996, DOE has declared ~50 metric tons (t) of Pu surplus to defense needs that requires disposition.[17,Box 2-2;35] DOE has already disposed 3.2 t surplus Pu in the form of residues and scraps in POCs at WIPP. In 2011, DOE decided to process 1.1 t of miscellaneous surplus Pu at Savannah River Site to meet WIPP acceptance criteria for CH-TRU by diluting it with an adulterant and disposing it at WIPP.[12] In 2016, DOE decided to dispose another 6.0 t of the non-pit Pu at WIPP and subsequently added it to the WIPP inventory for CRA-2019.[13]

DOE has also proposed to use the same processing to dispose an additional 34 t of surplus Pu waste at WIPP.[16;17] The additional 34 t of surplus Pu is considered in CRA-2026 and proposals to add seven additional panels to the WIPP repository.[14]

Because bounding estimates were used in 1996 CCA, and because estimates for CRA-2004 and thereafter greatly decreased the ^{239}Pu inventory, the disposal of 1.1 t and 6.0 t, as evaluated in CRA-2019, represents only a small increase in ^{239}Pu. Furthermore, the Pu fissile mass equivalence in CRA-2019 is still less than originally planned in 1996 (Table I). Disposing an additional 34 t of surplus Pu, as included in CRA-2026, greatly increases the ^{239}Pu inventory, but still does not cause a criticality concern after deposition in other areas of the repository or natural environment because Pu release from the WIPP disposal area is primarily sorptive or solubility controlled.[14;16;17]

Information Only

Table I. Projected fissile material at WIPP closure for selected certifications.

Radioisotope	1996[a] CCA[10] CH (kg)	1996[a] CCA[10] RH (kg)	CRA[b]-2004[36;37] CH (kg)	CRA[b]-2004[36;37] RH (kg)	CRA[c] -2009[38;39] CH (kg)	CRA[c] -2009[38;39] RH (kg)	CRA-2019[40] CH (kg)	CRA-2019[40] RH (kg)	RPPCR -23-19P[41;42] CH (kg)	RPPCR -23-19P[41;42] RH (kg)	CRA-26-12P[43] CH (kg)	CRA-26-12P[43] RH (kg)	CRA-26-19P[44;45] CH (kg)	CRA-26-19P[44;45] RH (kg)
Uranium														
^{233}U	860	16	130	3.5	16	5.3	11	1.8	41	14	32	1.7	37	13
^{234}U	75	6.9	45	6.0	49	0.83	77	1.6	106	3.1	104	1.1	118	3.2
^{235}U	5 900	2 100	610	440	2 000	33	2 100	860	1 171	918	750	541	807	945
^{238}U	120 000	31 000	73 00	390 000	81 000	880	117 000	9 300	342 520	9 833	285 300	5 263	321 230	10 400
Enrichment ^{233}U+^{235}U	4.9%	6.5%	1.0%	0.11%	2.5%	4.1%	1.8%	8.4%	0.35%	8.6%	0.27%	9.3%	0.26%	8.4%
Plutonium														
^{238}Pu	15	0.09	73	0.16	86	0.30	55	1.3	74	1.2	80	0.3	92	1.5
^{239}Pu	13 000	170	11 000	87	8 200	47	14 000	68	35 000	62	56 510	30	67 200	73
^{240}Pu	920	22	470	7.5	630	4.4	1 400	14	3 038	16	4 092	5.8	4 860	20
^{241}Pu	2.2	0.13	5.0	0.23	4.9	0.04	18	0.44	4.2	0.06	4.7	0.02	5.6	0.08
^{242}Pu	310	0.04	6.8	0.12	19	0.32	38	4.0	62	4.9	62	1.0	73	6.1
^{239}Pu fissile kg mass equivalent[d]	16 700	1 560[e]	11 200	370[e]	9 590	73.0	15 500	624[e]	35 900	670[e]	57 200	380[b]	67 900	697[b]
Enrichment ^{239}Pu	90%	88%	95%	92%	92%	90%	90%	78%	92%	74%	93%	81%	92%	73%

[a] EPA-requested PAVT-1997 for evaluating the 1996 CCA used the same inventory[46]
[b] Inventory masses were updated and differ somewhat for EPA-requested PABC-2004 analysis for evaluating CRA-2004[37]
[c] EPA-requested PABC-2009 analysis used the same inventory.[47]
[d] Pu fissile mass equivalence is the mass of ^{239}Pu plus factors for other fissionable masses: specifically, 0.113·^{238}Pu, 0.0225·^{240}Pu, 2.25·^{241}Pu, 0.0075·^{242}Pu, 0.9·^{233}U, 0.643·^{235}U, 0.015·^{237}Np, 0.0187·^{241}Am, 34.6·^{242m}Am, 0.0129·^{243}Am, 15·^{245}Cm, 0.5·^{247}Cm, 45·^{245}Cf, and 90·^{251}Cf. The factors derive from comparing the minimum critical mass of 0.45-kg ^{239}Pu (for a slurry, which includes bias and 0.02 margin on k_{eff}) to the minimum critical mass of other fissile isotopes.[48,Table XVI;49,§5.2]
[e] Pu fissile kg mass equivalence for RH-TRU primarily derives from 0.643 ^{235}U

II.A.3. TRU Containers

About 54% of CH-TRU is disposed in 7-packs of 55-gallon drums but CH-TRU also is disposed in 7-pack POC packages with a 12-inch inner vessel for CH-TRU waste (15%), standard waste metal boxes (8%), and 10-drum overpacks (4%). Super-compacted CH-TRU waste comes in 3-pack 100-gallon drums (19%). A few shipments have used 3-pack 85-gallon drums.[22, Table V]

For disposal in a salt repository, packaging allows for retrievability of the waste during operations. The packaging does not isolate the waste after closure of the salt repository. That is, none of the containers used at WIPP act as an engineered barrier to release in a brine environment. This paper focuses on conditions after substantial degradation of the containers. However, the container contents and packaging materials do influence the solubility of actinides and so some background information on containers is pertinent.

POC packages are composed primarily of steel and cellulose impact limiters. Future shipments of surplus Pu will likely come in CCO packages, which are constructed similar to POCs with a 6-inch inner criticality control container but without cellulose impact limiters (Table II). POC and CCO packages have increased the estimated iron mass in CH-TRU waste in the repository (Table III): Fe has increased from 49 110 t in 2014 to 63 130 t in 2019 and to 83 155 t in 2022 and cellulose mass from 4 391 t to 5 740 t to 8 839 t. The increase in Fe and cellulose mass increases the potential gas generation when sufficient brine is present (i.e., H_2 gas generation from steel corrosion and the CO_2 generation of biodegradation of cellulose).

Originally, all RH-TRU was to arrive in steel canisters and be emplaced in the repository walls (ribs). While some RH-TRU may still arrive in canisters, much RH-TRU waste may come in lead-shielded overpack containers and disposed in the excavated rooms in the future, which has greatly increased the Fe and Pb mass in RH-TRU containers (Table III).

Table II. Average iron mass emplaced in high-count payload containers by 31 December 2021.[50, Table 4]

Type	Count	Pkg (kg)	Content (kg)	Total (kg)
CCO	0	109.52	5.61	115.14
POC-12 inch	27 592	109.78	2.65	112.42
55 gal drum	108 900	28.2	6.34	34.54
100 gal drum	35 451	56.69	171.6	228.29
Ten drum overpack	6 960	816.9	308.14	1125.04
Standard waste box DL	7 070	295.97	228.71	524.52
Standard waste box OP	6 387	315.44	132.51	447.96

Information Only

Table III. Mass of major components of TRU waste in recent performance assessments.

Material	CRA-2019[40] CH (t)	CRA-2019[40] RH (t)	RPPCR-23[51] CH (t)	RPPCR-23[51] RH (t)	CRA-2026[44] CH (t)	CRA-2026[44] RH (t)
Waste						
Organics						
Cellulose	4 100	170	4 130	210	4 480	177
Plastics	5 320	414	5 700	313	5 610	305
Rubber	1 090	51.2	1 160	52.9	1 130	47.1
Solidified Organics	5 280	3.7	3 880	13.2	3 750	9.6
Inorganics						
Fe Metal	14 100	1 330	19 800	970	21 200	943
Al Metal	513	43.6	456	92.4	431	65.6
Other Metal	827	157	1 150	154	1 600	143
Solidified Inorganic	12 100	36.1	12 400	50.3	12 400	36.8
Other Inorganic	5 970	4 490	11 700	941	6 920	458
Cement	1 760	2.1	1 510	2.9	1 196	16.0
Soils	4 990	19.0	7 970	11.5	4 750	10.7
Waste Total	56 050	6 717	69 860	2 811	63 470	2 212
Packaging						
Cellulose	1 470	0	2 580	0	6 010	0
Plastic	2 830	468	3 680	942	4 610	1 090
Rubber	72.8	5.73	99.2	5.2	113	4.96
Lead	0	13 800	0	10 400	0	9 050
Steel Pkg	31 200	16 500	39 200	14 700	52 700	13 900
Pkg Total	35 500	30 800	45 560	26 050	63 430	24 040
Operation						
Cellulose	224		254		302	
Plastic	1 550		2 220		2 460	
Rubber	4.79		4.79		4.85	
Op Total	1 780		2 480		2 770	
Totals						
Fe	45 300	17 830	65 700	17 460	73 900	14 840
Cellulose	5 790	170	6 964	210	10 800	177
Plastic	9 700	882	11 600	1 260	12 680	1 400
Rubber	1 170	57	1 070	58	1250	52
*Cements**	8 880	3.5	8 740	4.3	8 590	17.4
Total Mat	93 330	37 460	117 900	28 860	129 670	26 250

*Cements are also included in solidified inorganic, solidified organic, and other inorganic material categories.

II.B. Geologic Characteristics of WIPP Disposal System

II.B.1. Castile Formation

The 500-m-thick Castile Formation, the lowest strata discussed here, consists of three anhydrite ($CaSO_4$) members and two interspersed halite (NaCl) members (Fig. 3). Within the land-withdrawal boundary of WIPP (Fig. 1), pressurized brine was intersected in the fractured Anhydrite III layer of the Castile by one exploratory borehole (WIPP-12) during site characterization (Fig. 1 and Fig. 3).[10, Appendix DEL, Section 7.5] The disposal area was moved 1.8 km south, but the presence of a brine source beneath the disposal area was not dismissed; hence, WIPP PAs assume (1) a potential pressurized brine source exists in the Castile beneath a portion of the repository, and (2) Castile brine could enter the repository through a new exploratory borehole in the next 10^4 years.

II.B.2. Salado Formation

The 600-m thick Salado Formation, which overlays the Castile Formation, hosts the WIPP repository 658 m below the surface. Near the repository (Fig. 4), the Salado Formation consists of nearly horizontal (<1° regional dip) halite (NaCl), argillaceous halite, and interbeds of clay and anhydrites ($CaSO_4$) of the Late Permian Period (~255 million years old or 255 Ma).[2, Fig. 4]

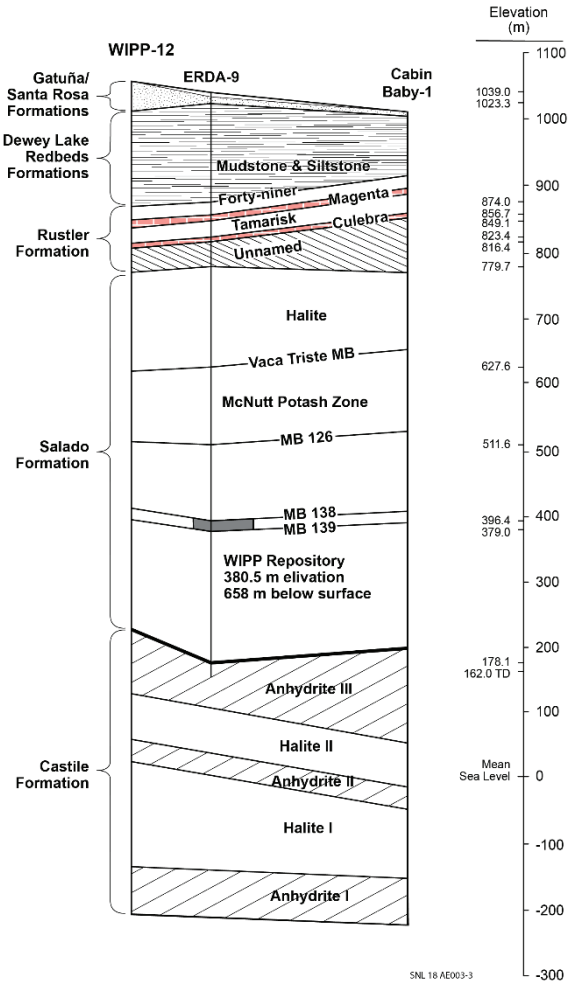

Fig. 3. Stratigraphy above and below the WIPP repository with elevation contacts referenced to ERDA-9.[2, Fig. 4;52]

Information Only

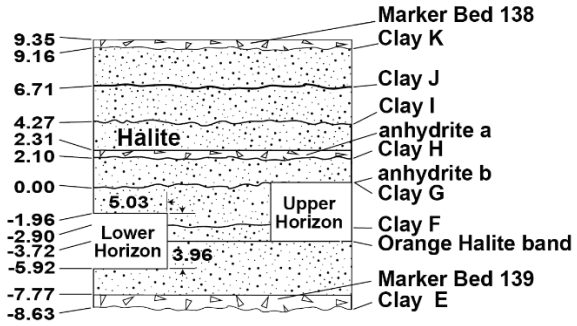

Fig. 4. Idealized model stratigraphy around WIPP disposal rooms in lower horizon (rooms in Panels 1, 2, 7, 8, and 10); and rooms in upper horizon (Panels 3, 4, 5, and 6) with elevations referenced to Clay G seam, which is at elevation 386 m, 652 m below surface at exploratory well ERDA-9.[52;53, Fig. 1]

II.B.3. Culebra Dolomite Member of Rustler Formation

The Rustler Formation overlies the Salado. The 7.3-m thick Culebra Dolomite Member, 216 m below the surface, is the most likely pathway for transporting radionuclides away from the repository after an inadvertent human intrusion because it is the most permeable saturated stratigraphic unit (Fig. 3).[5;9] The Culebra, consists mostly of dolomite with minor amounts of gypsum, quartz, and clay (Table IV).[26, Table II]

Table IV. Minerals in Culebra Dolomite strata.[26, Table II;28, Table II;54, p. 3-9]

Mineral (i)	Density (ρ_i) (kg/m^3)	wt %	vol %[a]
Culebra Dolomite			
Dolomite, $CaMg(CO_3)_2$	2840	91.5	90.71
Clay			
Corrensite $(Ca_{0.6}\ Na_{0.2}\ K_{0.2})(Mg_5\ Fe_3\ Al)(Si_6\ Al_2)O_{20}\ (OH)_{10} \bullet 9H_2O$	2800	2.4	2.41
Illite $(K_{0.6}(H_3O)_{0.4})\ (Al_{1.3}\ Mg_{0.3}\ Fe_{0.1})\ S_{3.5}\ O_{10}\ (OH)_2 \bullet H_2O$	2750	1.6	1.64
Gypsum, $CaSO_4 \bullet 2H_2O$	2320	3.0	3.64
Quartz, SiO_2	2650	1.5	1.59
Average grain density	2816		

II.C. Repository Design

In the original design of the WIPP underground facility, the excavated disposal region was divided into eight panels (of which 6 panels were filled at the beginning of 2014) plus two smaller panels composed of the 4 central connecting drifts (Fig. 5). However, in February 2014, a drum from Los Alamos National Laboratory burst when improperly filled with an organic rather than inert filler. ^{241}Am, ^{239}Pu, and ^{240}Pu were released that contaminated some of the underground. [55]

DOE has abandoned the southern equivalent panel and closures between Panels 3, 4, 5, and 6 in the southern portion of the repository to avoid undue worker exposure. To accommodate the lost space, at least two replacement panels and up to nine panels may be excavated to the west of existing panels along drifts to the north of Panel 8 (Fig. 5). The expansion does not change the maximum TRU waste volume of 175 564 m^3 (6.2×10^6 ft^3) authorized for disposal in the *Waste Isolation Pilot Plant Land Withdrawal Act*.[3]

A full panel is divided into 7 rooms. A room has volume of 6585 m^3, including the connecting drifts to form a square bracket shape. Ideally 10 908 55-gallon drums can be placed per room. Although some rooms in Panels 1 through 4, might have up to 7.9% of the disposal room volume backfilled with bags of magnesium oxide (MgO), the current average in Panels 5, 6, and 7 is ~3.5% (Table V).[22, Table VI] Thus, a 1905 kg polypropylene sack of MgO is typically placed on every other column of containers in a current room (Fig. 5). MgO acts as a buffer to control pH of any brine that seeps into the rooms prior to waste encapsulation. The MgO also combines with any CO_2 formed during degradation of organic matter, such that highly soluble Pu and U carbonate species are not formed.[22]

Table V. MgO mass and volume emplaced in WIPP Rooms

	Room-Segment MgO Mass per 7 Rooms in a Panel[a,b] (metric tons—t)		
Panel	**Ave**	**Max**	**Min**
1	354	624	123
2	527	569	383
3	508	566	367
4	512	581	370
5	416	518	269
6	260	411	130
7	149	307	32
Overall	389	624	32
Panels 5,6,7	275	518	32
	Porous Volume[c] (m^3)		
Overall	180 (4.9%)	289 (7.9%)	15 (0.4%)
Panels 5,6,7	127 (3.5%)	240 (6.6%)	15 (0.4%)

[a] Query of the WIPP Waste Data System on 3 August 2023
[b] Adjusted by ratio of full volume to straight segment volume (i.e., 6585m^3/3642 m^3)
[c] Assumes 3600 kg/m^3 grain density and 40% MgO porosity

Information Only

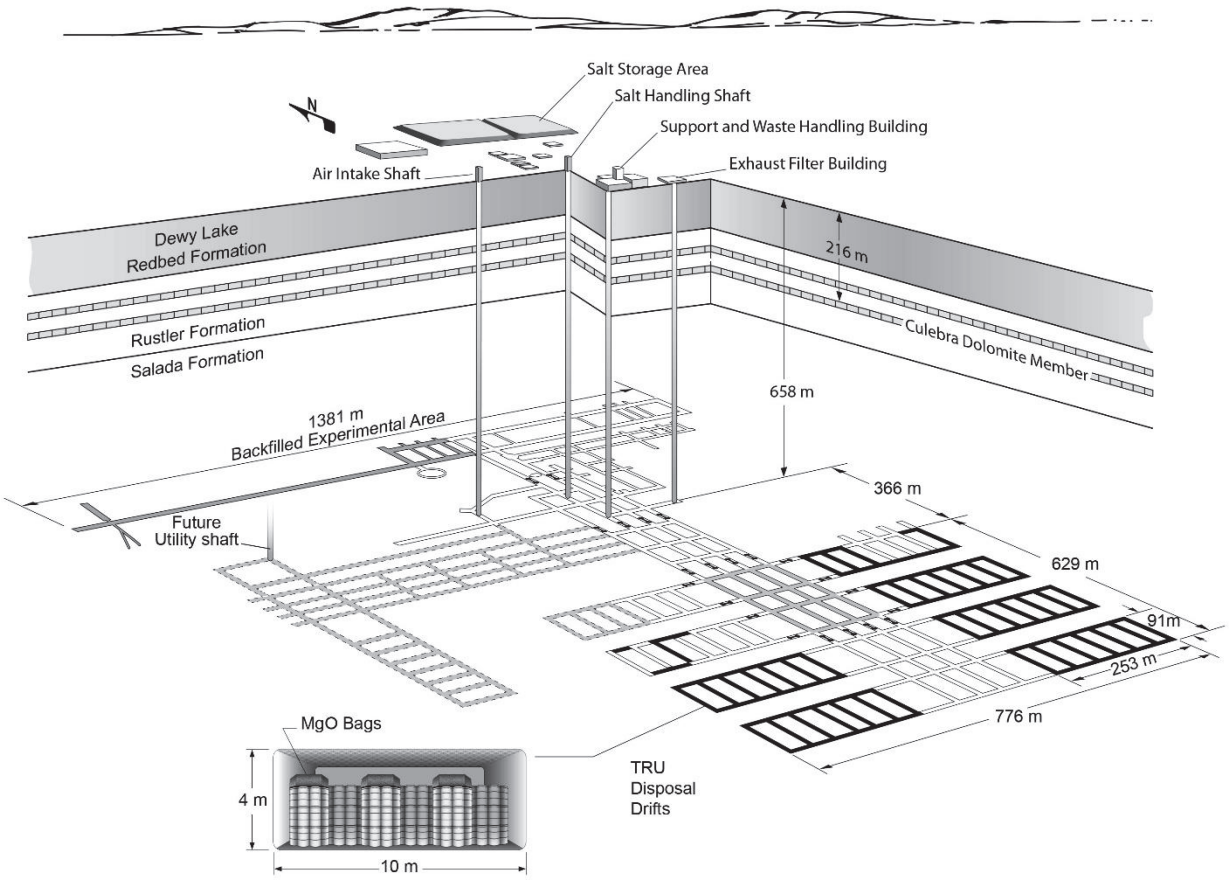

Fig. 5. Transuranic waste disposal area of the WIPP repository has 8 panels and one equivalent panel in the north central region; EPA has authorized 2 replacement panels to the west;[15] 7 additional panels have also been proposed to the west.[14]

III. NEUTRONIC CONSTRAINTS

III.A. Critical Mass and Concentration in Mixtures of Brine and Geologic Media

The criticality mass and asymptotic concentration limits used herein are based on modeling mixtures of water, salt, dolomite, concrete, rust, and fissile material using a neutron/photon transport computational code. In a neutronic report,[28] several idealized depositional spheres of fissile material homogeneously mixed with fluids and geologic media were analyzed. Substituting WIPP brines for water substantially increases the mass of fissile material necessary to go critical for both ^{239}Pu and ^{235}U. The addition of geologic media to a fissile/water binary system also substantially increases the mass of fissile material necessary to go critical (Fig. 6 and Fig. 7).

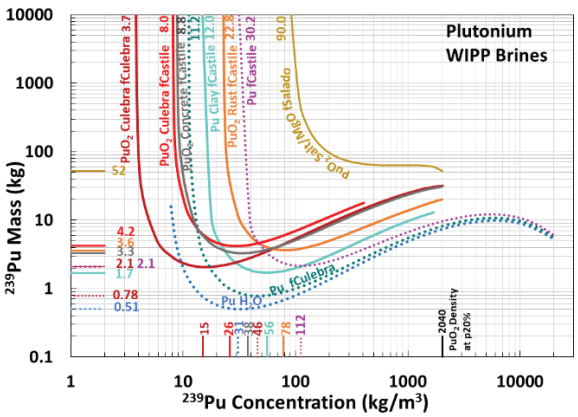

Fig. 6. Critical mass and concentration limits for homogeneous spherical shape of Pu in various materials at 20% porosity saturated with WIPP brines.[26, Fig. 35;28, Fig. 28]

Information Only

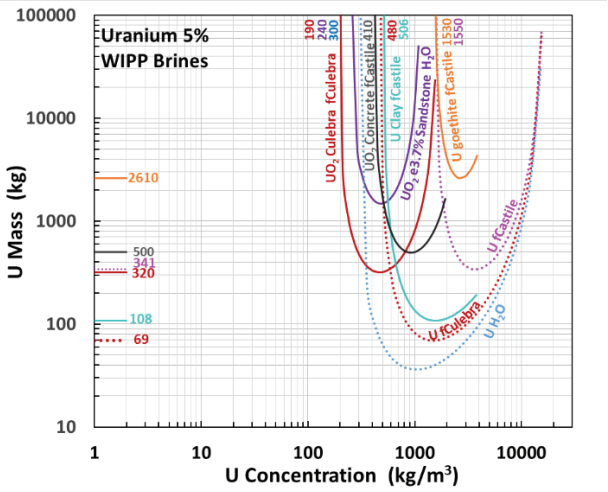

Fig. 7. Criticality limits for 5% enriched ^{235}U deposited in homogeneous spherical shape in various material at 20% total porosity saturated with WIPP brines.[26, Figs. 34&36;27, Fig. 6;28]

Criticality limits are determined for three compositions of WIPP brines: Castile, Salado, and Culebra (Table VI). The Culebra brine composition is based on measurements at the air intake shaft (where Culebra fluid is technically a saline water since total dissolved solids of~43 kg/m^3 is between 30 and 50 kg/m^3) The Castile brine composition is based on early exploratory borehole ERDA-6 (Table VI).[56-58]

Table VI. Composition of Culebra, Salado, and Castile brines near WIPP.

Constituent	Concentration (mM or mole/m^3) Culebra (Air Shaft)[a]	Salado (Weeps)[b]	Castile (ERDA-6)[c]
Sodium (Na^{+1})	600	3530	4870
Magnesium (Mg^{+2})	21	1020	19
Potassium (K^{+1})	8.3	467	97
Calcium (Ca^{+2})	23	14	12
Boron ($B(OH)_4^{-1}$)	2.8	158	63
Chloride (Cl^{-1})	567	5860	4800
Sulfate (SO_4^{-2})	77	177	170
Bromine (Br^{-1})	0.37	27	11
Bicarbonate (HCO_3^{-1})	1.1	16	16
Ionic strength	800	6700	5300
pH	7.7	7.0	7.0
Total solids (kg/m^3)	42.	368	313
Density	1040	1237	1201

[a]Sampled at air intake shaft[56]
[b]Synthetic approximation of intergranular fluids of Salado Fm.[59]
[c]Synthetic approximation of well drilled to Castile Fm.[60]

The intergranular Salado brine composition, based on weeps measured at the repository horizon has substantially more magnesium, potassium, chloride, and boron than Castile brine (Table VI). The chloride and boron are particularly important for the post-closure criticality evaluation and so criticality limits for both Castile and Salado brine have been reported but values for the more reactive Castile and Culebra brines are reported here.

The porosity of the geologic media has a strong influence on both the critical mass and the critical concentration in WIPP brines (and H_2O). As the porosity increases, the behavior approaches that of a fissile/fluid binary system, along with a decrease the critical mass. (e.g., Pu/Culebra dolomite/Culebra brine approaches Pu/Culebra brine system as porosity increases in Fig. 6).

The corresponding critical spherical radius for PuO_2 somewhat plateaus between 100 and 1000 kg/m^3 (Fig. 8) but does not have a minimum until the porosity is filled. In contrast, UO^2 at 5% enrichment in various material have minimums that place geometric constraints on criticality (Fig. 8).

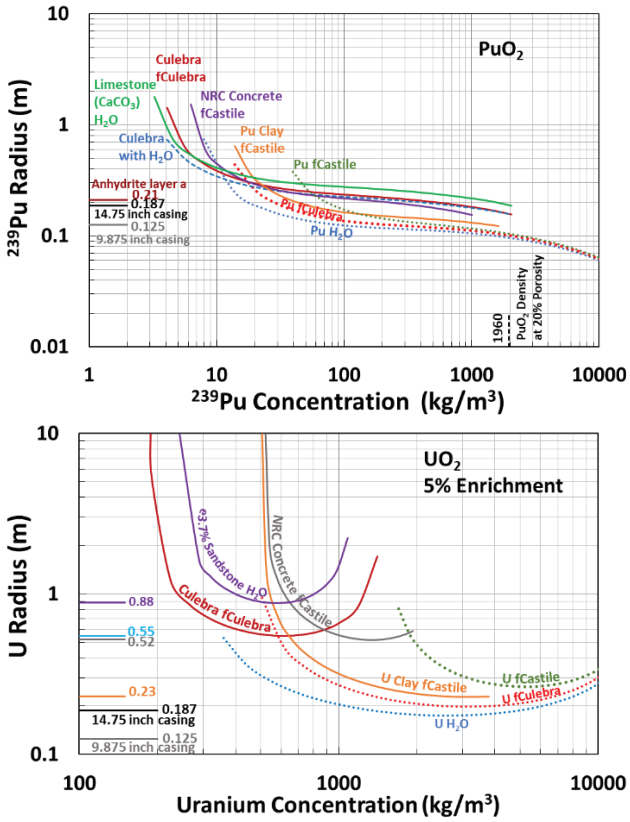

Fig. 8. Critical radius for PuO_2 and UO_2 in various media with 20% porosity filled with water and WIPP brines data.[26, Figs. 37&38;28])

The influence of geologic media on the asymptotic limiting concentration varies. For geologic media primarily composed of elements with large neutron absorption cross-sections in the thermal region such as iron in rust or chloride in salt, the geologic material

Information Only

increases the critical asymptotic concentration compared to the fissile/water binary system. For geologic media primarily composed of elements with small thermal cross-sections such as silicon, the geologic material decreases the critical asymptotic concentration.

The advective porosity of the Culebra dolomite is primarily along bedding planes and fractures. The matrix porosity may be inaccessible except by diffusion; thus, fissile deposition may only occur in the fracture porosity. A companion report evaluated heterogeneity effects, and the found that a saturated heterogeneous system with highly enriched ^{239}Pu or highly enriched ^{235}U is never more reactive than a saturated system. It is possible to find a low enriched heterogenous system with large fracture porosity and small fracture spacing that is more reactive than a corresponding homogenous system, but the fracture porosity is larger and the advective fracture spacing smaller than occurs in Culebra dolomite near WIPP (Fig. 9).

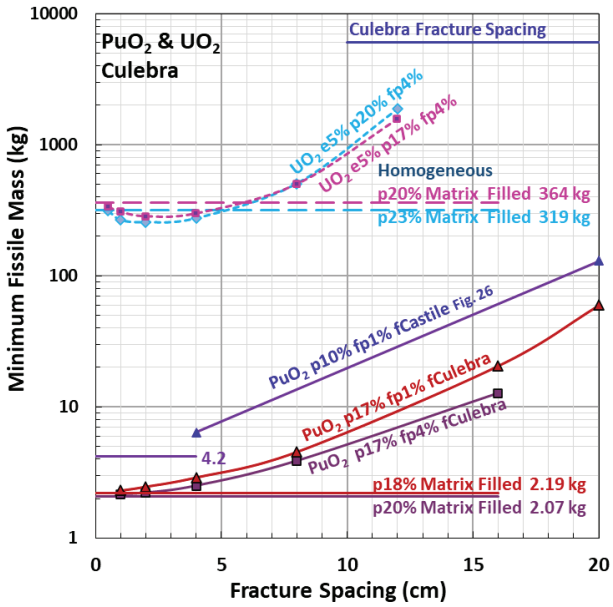

Fig. 9. Homogeneous system of ^{239}Pu and ^{235}U is always more reactive than heterogeneous system for fracture spacing occurring in Culebra dolomite.[26, Fig. 29;28, Fig. 26]

III.B. Geometric Constraints on Deposition in Anhydrite Layers and Boreholes near Repository

Intrusion boreholes do not have sufficient space to contain a sphere of ^{235}U. Currently at the Culebra horizon, oil and gas wells are using 14 ¾ inch casing (0.187 m radius). At the repository horizon, oil and gas wells are using 9 $^{7/8}$ inch casing (0.125 m radius). To have sufficient space to have criticality and avoid excessive neutron leakage, a borehole filled with fractured concrete, requires a radius of 0.52 m; a borehole filled with Culebra dolomite and Culebra brine requires a radius of 0.55 m, and a borehole filled with clay and Castile brine requires a radius of 0.23 m. All dimensions are larger than the 9 $^{7/8}$ inch and 14 ¾ inch casing (Fig. 8).

Similarly, most anhydrite layers ($CaSO_4$) within 20 m of the repository horizon, are thin and have insufficient thickness to contain a 0.5-m diameter sphere of ^{235}U. From Fig. 4, Marker Bed 138 is 0.19 m thick, and Anhydrite "a" is 0.21 m thick. The only exception is the ~0.9-m thick Marker Bed 139 directly below the repository. In MB 139, hydrologic conditions do not favor substantial movement of brine carrying dissolved Pu, as noted in §IV.A below.

III.C. Regulatory Constraint at Disposal System Boundary

The Individual Protection Requirement in 40 CFR 191 at the accessible environment is 0.15 mSv/y, which is equivalent to ~78 pCi/L for ^{235}U and ~5.5 pCi/L for ^{239}Pu.[c] In turn, the 5.6 pCi/L for ^{239}Pu is ~4×10^{-10} mM,[d] which is 10 orders of magnitude less than that required to go critical (i.e., 4.7 mM or 11.2 kg/m^3 for Pu in Culebra brine—Fig. 6). The Ground Water Requirement in 40 CFR 191 at the accessible environment is more stringent for ^{235}U—15 pCi/L. The equivalent radioisotope concentrations of 15 pCi/L for ^{235}U is 3×10^{-5} mM, which is 8 orders of magnitude less than required to go critical (i.e., 2040 mM or 480 kg/m^{3}in Culebra brine—Fig. 7). Hence, if the Individual Protection and Ground Water Requirements are met, there is insufficient concentration to cause criticality near the boundary of the accessible environment

IV. DISSOLVED FISSILE CONCENTRATION

IV.A. Solubility Model and Oxidation State Analogy

The baseline solubility for an actinide is calculated using a chemical equilibrium code. For the CCA, FMT, a code specifically written for tWIPP, was used.[62] After CRA-2014, EQ3/6 v 8.0a was used.[63] Both codes access the WIPP database of Pitzer interaction coefficients for high-ionic strength solutions, such as Castile and Salado brines. For CRA-2019, DATA0.FM1 version was used.[64]

[c] The calculation assumes drinking 2 L/d of water is the sole source of exposure: 0.15 mSv/y •2 L/d • f^{ingest} • 2.7×10^{-3} d/y where f^{ingest} is the ingestion dose factor[61] and equal to 1.4×10^{7} Bq/Sv for ^{235}U and 10^{6} Bq/Sv for ^{239}Pu and conversion factor is 2.7×10^{-11} Ci/Bq.

[d] The calculation is as follows: 5.6 pCi/L/(w_{239Pu}•m_{239Pu}) where w_{239Pu} is the activity conversion factor of 6.2×10^{-2} Ci/g and m_{239Pu} is the molecular weight of ^{239}Pu.

Information Only

The solubility of plutonium is difficult to assess because it can readily change from either Pu^{3+}, Pu^{4+}, Pu^{5+}, or Pu^{6+}, and is often present as a combination of several of these oxidation states in experiments. However, experimental evidence suggests that actinide elements in the same oxidation state exhibit the same chemical behavior ("oxidation state analogy");[65;66;67, p.536] thus, it is possible to use Pitzer coefficients experimentally evaluated for other actinides. Pitzer coefficients evaluated for Am^{3+} are used to estimate the solubility of other 3+ actinides such as Pu^{3+}. Pitzer coefficients for Th^{4+} are used for other 4+ valence actinides such a Pu^{4+} and U^{4+}.

Except for the changes between the 1996 CCA and EPA performance assessment verification test (PAVT) the changes have been gradual. Finding Pitzer coefficients for the 1996 CCA was challenging. For example, a Pitzer coefficient for interaction of carbonate species of 4+ actinides with Cl^{-1} was unavailable for the 1996 CCA. However, a Pitzer coefficient for $Th(CO_3)_5^{-6}$ interacting with Cl^{-1} was measured shortly thereafter that reduced the solubility of 4+ actinides by 2 orders of magnitude for the PAVT-1997 (Fig. 10).[2]

IV.B. Oxidation State Dependence

Actinides present in the WIPP inventory can exist in the 3+, 4+, 5+, or 6+ oxidation states. The higher oxidation states (5+ and 6+) are more soluble than lower oxidation states (3+ and 4+), except within the latter group, 3+ actinides are more soluble than 4+ actinides. Although plutonium can be present as either Pu^{3+}, Pu^{4+}, Pu^{5+}, or Pu^{6+}, or often as a combination of several of these oxidation states, the WIPP project reasons that plutonium would exist as Pu^{3+} and Pu^{4+}, because of the ubiquitous presence of iron from TRU waste containers (several thousand times the amount of metallic iron necessary to convert Pu^{6+} to Pu^{4+}), as shown in experiments under anoxic conditions with WIPP brines. Hence, the mass of iron is an important input for the chemical equilibrium solubility model (i.e., ~73 900 t iron in CH-TRU waste packages and ~14 800 t iron in RH-TRU waste packages in CRA-26-19P—Table II).

Other metals in the waste are also able to reduce the actinides, but only lead used in shielded RH-TRU containers is present in sufficient quantity to include in the solubility model (i.e., 9050 t in CRA-26-19P—Table II)

The WIPP Project assumes that chemical conditions in RPPCR/CRA-2026 cause plutonium and uranium to have +4 valence (Pu^{4+}) in 75% of the stochastic samples, based on recent experimental work, irrespective of the inventory (since the large mass of surplus Pu would be disposed as PuO_2 at +4 valence). In the other 25% of samples, plutonium exists as +3 valence (Pu^{3+}).[14] Up through CRA-2019, the stochastic split was even: 50% +3 valence and 50% +4 valence.[65] When Pu^{3+} is present, then U^{4+} is present; when Pu^{4+} is present then U^{6+} is present.

IV.C. Brine Dependence

The range of dissolved Pu and U solubility (S^D) is somewhat dependent upon the ionic strength (i) (i.e., type of brine). Consequently, the solubility is estimated for both Salado (i = 6700 mM) and Castile brines (i = 5300 mM) in analyses (Fig. 10). In the 1996 CCA, the solubility of both 3+ and 4+ actinides (e.g., Pu^{3+} and Pu^{4+}) differed substantially in Castile and Salado brines (Fig. 10). The most striking result since CRA-2004, however, is that though the 3+ and 4+ actinide solubility still differ, they behave similarly in Castile and Salado brines (Fig. 10), because the iron/lead in containers produce similar redox conditions and the added MgO backfill prevents formation of carbonic acid ($H_2CO_3^*$).

IV.D. Brine Mixing Volume

The chemical equilibrium solubility model is not coupled into the PA simulation. Rather, PA simulations interpolate between solubilities determined at 5 brine volumes: a minimum brine mixing volume (based on the minimum brine volume for which a direct brine release to the surface is possible after a drilling intrusion in each certification) and a factor of 2, 3, 4, and 5 times the minimum brine volume.[59] For CRA-2009, CRA-2014, and CRA-2019, the minimum mixing volume was 17 400 m^3 in disposal rooms.[68] For RPPCR-23-19P, the minimum mixing volume was 33 800 m^3, because of 9 additional panels.[69] For CRA-2026, the minimum mixing volume is 9 608 m^3.[70] CRA-26-19P considers 9 additional panels, but the factor of 3.5 decrease in the mixing volume is because of the decrease in porosity as the room closes from salt creep as evaluated for CRA-2026.[71]

IV.E. Organic Ligand Concentration

Organic compounds can form strong complexes with actinide ions, thereby stabilizing and increasing the actinide concentration in the solution. Of the ~60 organic compounds in TRU waste,[72;73] four influence actinide solubility because they are water-soluble and present in significant quantities: acetate, citrate, oxalate, and ethylene diamine tetra-acetate (EDTA). The projected masses of the four organic ligands in each WIPP certification dissolved in the brine mixing volume are used in the chemical equilibrium solubility calculations.[40;44]

IV.F. pH Dependence and MgO Control

The pH (i.e., activity of hydronium ion $[H^+]$) of the solution greatly influences the solubility of Pu and U. For WIPP, enough MgO is placed in the repository such that any CO_2 generated by microbial degradation of organic material in the waste forms hydromagnesite,

Information Only

$Mg_5(CO_3)_4(OH)_2 \bullet 4H_2O$, and does not dissolve into the brine to form carbonic acid (H_2CO_3*). The acid would lower the pH to ~4.5. With MgO, the pH of the brine stays within the range of 8.8 to 9.0 in the disposal area. Narrowing the pH range narrows the radioisotope solubility range.

Hence, the reacted mass of hydromagnesite, and the mass of the hydrated MgO precursor, brucite ($Mg(OH)_2$), are compounds in the chemical equilibrium solubility model. In turn, the masses of cellulose, plastics and rubber in containers are necessary to determine the MgO mass placed in the disposal area[22, Eq. (1)] (e.g., 10 790 t of cellulose and 12 680 t of plastics, and 1 095 t rubber forecast in CRA-2026—Table II).

The mass (m_{MgO}) placed in the WIPP disposal region (Table III) is calculated assuming a one-to-one correspondence between CO_2 produced and six times mass of carbon in waste cellulose (m_{cell}) ($C_6H_{10}O_5$), rubber (m_{rub}), and factor of 1.7 times mass of plastics (m_{plstc}) with a safety factor (f_{MgO}^{safety}):[74;75]

$$m_{MgO} = 6 f_{MgO}^{safety} \left(m_{cell} + m_{rub} + 1.7 m_{plstc} \right) \bullet \frac{40.3 \text{g/mole MgO}}{162 \text{ g/mole cellulose}} \quad (1)$$

After February 2008, f_{MgO}^{safety} has been set at 1.2.[76]

CCOs containing surplus Pu have only a small amount of plastic used to bag the handling cans to reduce the possibility of Pu contamination in the packaging facility. For 0.40 kg polyethylene per CCO and 15.2 kg of plywood per CCO, 28.4 kg of MgO per CCO is required.

IV.G. Actinide Solubility at Minimum Brine Mixing Volume

The baseline solubility of Pu^{4+} at the minimum brine volume has remained fairly stable since CRA-2004: within 12% in Salado brine (e.g., 5.3×10^{-5} mM for S_{CRA26}^{Base}(4+,Salado,minVol) and 6.0×10^{-5} mM for S_{CRA14}^{Base}(4+,Salado,minVol)) and within 30% in Castile brine (e.g., 5.7×10^{-5} mM for S_{CRA26}^{Base}(4+,Castile,minVol) and 4.2×10^{-5} mM for S_{CRA14}^{Base}(4+,Castile,minVol)) The baseline solubilities of Pu^{3+} have varied more but still within an order of magnitude between CRA-2004 and RPPCR-23 (e.g., 3.4×10^{-3} mM for S_{CRA19}^{Base}(3+,Salado,minVol) and 3.9×10^{-4} mM for S_{CRA04}^{Base}(3+,Salado,minVol)). The large decrease in mixing volume for CRA-2026 (§V.C) has caused a large increase in Pu^{3+} 1.1×10^{-2} mM for S_{CRA26}^{Base}(+III,Salado,minVol)) (Fig. 10).

IV.H. Uncertainty in Solubility.

The interpretated solubility uncertainty has fluctuated and accounts for much of the changes in mean solubility observed since CRA-2004 (Fig. 10). Uncertainty in solubility is dependent on the uncertainty of the brine chemistry, but this brine chemistry is not evaluated in the PAs. The uncertainty about the FMT and EQ3/6 calculated baseline dissolved concentration ($S_{CCA96}^{Base}(Ox)$ was estimated using a sampled scale factor (10^{f_D}). For the 1996 CCA and PAVT-1997, a piece-wise linear distribution of f_D was set by analyst judgement that varied 3.4 orders of magnitude. Specifically, the range was $-2 \le f_D \le 1.4$ with mean of 0.18 and median of -0.09.[57, Table 12;77,p. 5-15] Although the same distribution was used for Pu and U oxidation states and Castile and Salado brines, the distribution was sampled separately without correlation (Fig. 10).

For CRA-2014, the uncertainty distribution was a function of the oxidation state (i.e., $10^{f_D(Ox)}$) and established through comparison of a wide range of measured values and predictions from EQ3/6 for 3+ and 4+ actinide oxidation states (Fig. 10). The distribution varied 6.5 orders of magnitude for Pu^{3+}; specifically $-3.55 \le f_D(3+) \le 2.97$.[57, Table 12] The distribution varied 4.7 orders of magnitude for Pu^{+IV}; specifically, $-1.52 \le f_D(4+) \le 3.19$.

For CRA-2019, the distribution of $f_D(Ox)$ was based on a reduced set of experimental values based on 10 inclusion criteria.[e] The uncertainty distribution for the Pu^{4+} and U^{4+} was similar to the 1996 CCA and PAVT-1997 (3.4 orders of magnitude variation or $-2.01 \le f_D(4+) \le 1.43$). The uncertainty distribution varied 4 orders of magnitude for Pu^{3+} (Fig. 10) or $-1.14 \le f_D(4+) \le 2.97$.

Uncertainty analysis continued to be refined for RPPCR-23/CRA-2026. The uncertainty distribution for the Pu^{4+} and U^{4+} is less than the 1996 CCA (2.5 order of magnitude variation or $-2.01 \le f_D(4+) \le 0.53$). The

[e] The 10 criteria specified inclusion of results from studies that [78;79] (1) preferably published after 1990; (2) published in journals, official government laboratory reports, unpublished theses; published industry studies; (3) evaluated solubility (not corrosion, sorption, etc.), (4) used water as solvent; (5) were conducted at atmospheric pressure and WIPP temperatures—20 to 30 ºC; (6) evaluated Th^{4+}, Nd^{3+}, Am^{3+}, and Cm^{3+}, not studies of U^{4+}, Np^{4+}, Pu^{3+}, and Pu^{4+} because of difficulty in maintaining oxidation state of U, Np, Pu; (7) well-characterized solubility-controlling solid available in WIPP thermodynamic database; (8) used dissolved species available in the WIPP thermodynamic database; (9) described experiments, not studies summarized in literature reviews, sufficient to be repeatable and allow computer simulation; and (10) used conditions similar to WIPP, that is, $0 \le Mg \le 1600$ mM; $0 \le Ca \le 500$ mM; 5 molality≤ionic strength≤9.5 molality; total inorganic carbon ≤ 20 mM; and $8 \le pcH \le 10.7$).

Information Only

uncertainty distribution for Pu^{3+} for CRA-2026 is now similar to the 1996 CCA based on analyst judgement (3.4 order of magnitude variation or -2.76 ≤ $f^{D}_{RPPCR23}(4+) \le 0.598$) (Fig. 10).

Based on the uncertainty distribution, the mean and median values were also adjusted from the baseline solubility (e.g., $\overline{S}^{D}_{CRA26}(3+,\text{Salado,minVol}) = 3.69\times10^{-5}$ $=10^{-0.49}S^{\text{Base}}_{\text{CRA26}}(3+,\text{Salado,minVol})$).

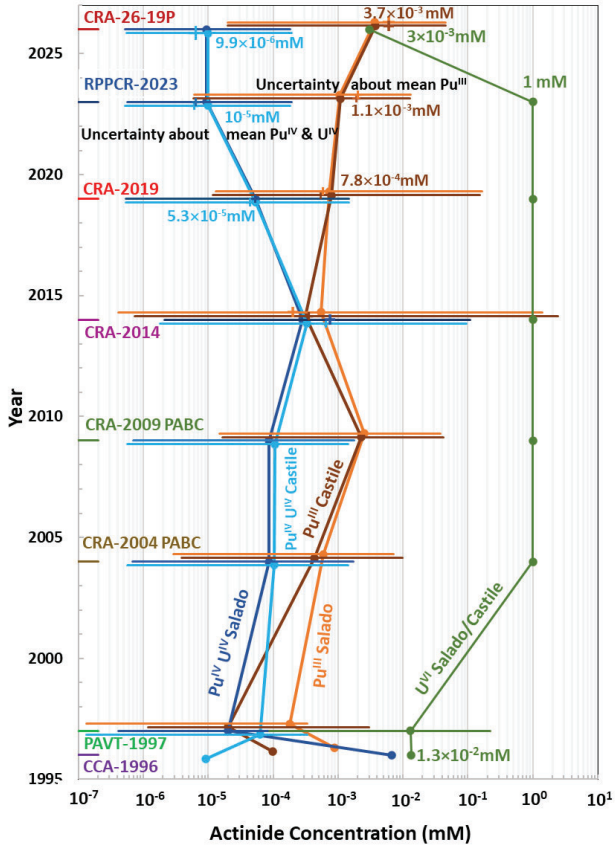

Fig. 10. Mean, median, and range of actinide dissolved solution concentration (without colloids) for 3+,4+, and 6+ oxidation states in disposal rooms at minimum brine mixing volume for WIPP certifications.[CRA-2026,Table GEOCHEM-26]

IV.I. Comparison of Criticality Limits to Dissolved Concentration

The asymptotic criticality concentration limit of 30.2 kg/m^3 for ^{239}Pu in Castile brine (Fig. 6) corresponds to 130 mM. This critical concentration is 4.5 to 5.2 orders of magnitude greater than the mean Pu^{3+} dissolved concentration of ~3.7×10^{-3} mM in CRA-2026 and 7.8×10^{-4} mM in CRA-2019.

The maximum dissolved $^{239}Pu^{3+}$ concentration of 0.17 mM in Castile brine in CRA-2019 (i.e., $10^{f_D} \bullet S^{Base}_{EQ/6,Pu^{+3}} = 933 \bullet 1.8 \times 10^{-4}$ mM—Table VI) is 3 orders of magnitude below the limit necessary to create a critical solution of ^{239}Pu in Castile brine (i.e., 0.17 mM or 0.04 kg/m^3 versus 30.2 kg/m^3—Fig. 6) and 2 orders of magnitude greater than the maximum Pu^{3+} solubility in CRA-2014 (Fig. 10).

Also, the asymptotic criticality concentration limit of 1550 kg/m^3 for ^{235}U in Castile brine (Fig. 7), corresponds to 6.6×10^3 mM, a concentration almost 4 orders of magnitude greater than the maximum $^{235}U^{VI}$ concentration of 1 mM (0.24 kg/m^3) ever used in WIPP analysis (Fig. 10).

V. COLLOIDAL FRACTION

Colloids typically have sizes of between 1 nm and 1 µm. Colloid formation and stability depend on their composition and the prevailing chemical conditions (e.g., ionic strength). Depending on their size, colloid transport may occur at different rates than fully dissolved species. They may be physically excluded from fine porous media, and their migration may be accelerated through fractured media in channels where velocities are greatest. Colloids can also interact with the host rock during transport and become retarded. These interactions may be of a chemical or physical nature and include electrostatic effects leading to colloid sorption or sieving leading to colloid filtration. [13, App. SCR, FEPs W79, W80, W81]

V.A. General Fate of Colloids in Rooms prior to Intrusion

The behavior of the colloidal particles themselves is best described as a steady-state process, in which new particles are continuously generated and dispersed in the liquid phase but are gradually destabilized through a variety of processes. Destabilization of mobile colloidal fissile actinides, followed primarily by gravitational settling, could conceivably concentrate fissile material, but the mechanism is limited to local microenvironments that are likely to be centimeter-sized or even smaller within the WIPP repository.

Room closure through salt creep will crush the waste containers and compact the waste material. Colloidal particles could form throughout the waste matrix; however, the fluid columns in which agglomerated colloidal particles will settle are likely to be short and poorly connected. Consequently, the local concentrations of colloidal agglomerates that develop in the WIPP will remain uniformly distributed in the waste throughout the repository and will not concentrate in a single location. By analogy to a closed house, dust (i.e., aerosols) settles on the horizontal surfaces in the house. The dust does not readily concentrate at a single location.

Information Only

V.B. General Constraint on Colloidal Filtration in Repository after Intrusion

In a disturbed repository, flowing brine could result in filtration of dispersed colloidal actinides, but concentration of colloidal actinides will again be localized in small microenvironments. As described above, the waste will contain many centimeter-sized microenvironments of small poorly connected pores. Filtration can take place in interstices at the boundaries of marked changes in pore size, resulting in small concentrations of colloidal actinides in those localized small areas.

Again, considering the dusty-house analogue, an air stream flowing through an open house is similar in concept to brine flowing through the repository. In the dusty house, dust that has settled on horizontal surfaces is stirred up and concentrated in local environments, such as corners or other areas where horizontal air velocity is small. In the repository, local accumulations will develop in a similar fashion. However, the tight packing of the waste will provide local filtration of colloidal particles. Hence, the fissile actinides associated with colloidal particles will remain fairly uniformly distributed within the repository on a macroscopic scale.

V.C. Colloidal Fraction of Total Fissile Concentration

The concern with colloids is (1) whether the concentration of colloids is critical or (2) whether there is a mechanism by which actinide-bearing colloidal particles can be locally concentrated through aggregation or filtration. Like sorption (§VI), the uptake of fissile actinides by the various types of colloidal particles is governed by equilibrium among dissolved actinides, solid actinide phases, and the colloidal particles. The link between colloidal actinide concentration and equilibrium thermodynamics produces a limit on the concentration of colloidal actinides that cannot reasonably exceed by orders of magnitude the fissile dissolved concentration and thereby go critical as follows.

Four categories of actinide colloids are considered at WIPP: mineral, intrinsic, humic, and microbial.[58] Humic colloids are actinides complexed by humic organics; microbial colloids are microbes that have sorbed actinides; mineral-type colloids are mineral substrates that readily sorb actinides; and intrinsic colloids are polymeric radioisotopes. The mineral colloid concentration ($C^{mineral}$) was fixed at 2.6×10^{-5} mM.[80] In the 1996 CCA, only Pu^{4+} was assumed to form intrinsic colloids at a fixed concentration (C^{int}_{4+}) of 4.3×10^{-5} mM.[81] For CRA-2019 and CRA-2026, C^{int}_{4+} is still fixed at 4.3×10^{-5} mM, but C^{int}_{3+} is fixed at 9.5×10^{-6} mM.[81] Also, other actinides (Am, Th, U, and Np) can also form intrinsic colloids.[13, Table GEOCHEM-61]

The concentration of humic colloids was assumed to be a fraction of the dissolved concentration ($S^{D}_{Ox,Br}$), which is a function of the oxidation state (Qx) and ionic strength and, thus, brine type [Br] (i.e., $C^{humic}_{Ox,Br} = f^{humic}_{Ox,Br} \bullet S^{D}_{Ox,Br}$). The humic colloidal concentration was bounded by 0.011 mM.[82]

Experiments with WIPP-relevant microbes found that microbes do not actively move actinides through the cell membrane, but instead passively adsorb actinides extracellularly similar to mineral sorption.[83] Hence, the microbial colloidal concentration is only a fraction of the dissolved concentration ($S^{D}_{Ox,Br}$) (i.e., $C^{microbe}_{Ox,Br} = f^{microbe}_{Ox} \bullet S^{D}_{Ox,Br}$)

For PA modeling of actinides releases from the disposal area to the surface after an inadvertent intrusion (i.e., direct brine releases), the total actinide concentration is calculated as the sum of the dissolved species ($S^{D}_{Ox,Br}$) and the four categories of colloids, The calculation is as follows (Table VII):[13,Appendix GEOCHEM;65, Table I]

$$ {}^{uncrt}C^{T}_{Ox,Br} = {}^{uncrt}S^{D}_{Ox,Br} + {}^{uncrt}C^{humic}_{Ox,Br} + {}^{uncrt}C^{microbe}_{Ox} + C^{mineral} + C^{int}_{r} \quad (2) $$

where

$$ {}^{uncrt}S^{D}_{Ox,Br} = 10^{f^{D}_{uncrt,Ox}} S^{BaseEQ3/6}_{Ox,Br} $$

$$ {}^{uncrt}C^{humic}_{Ox,Br} = \min \begin{cases} f^{humic}_{Ox,Br} \bullet {}^{uncrt}S^{D}_{Ox,Br} \\ 1.1\times10^{-2}\ \text{mM} \end{cases} $$

$$ {}^{uncrt}C^{microbe}_{Ox,Br} = \min \begin{cases} f^{microbe}_{Ox} \bullet {}^{uncrt}S^{D}_{Ox,Br} \\ L^{Cap}_{Ox,r} \end{cases} $$

$$ C^{mineral} = 2.6\times10^{-5}\ \text{mM} $$

$$ C^{int}_{Pu} = 4.3\times10^{-5}\ \text{mM} $$

$$ C^{int}_{U} = 1.4\times10^{-3}\ \text{mM} $$

For CRA-2019, $L^{MicroCap}_{Ox,r}$ was set at 3.8×10^{-5} mM for radionuclides at all oxidation states. For CRA-2026, $L^{MicroCap}_{Pu^{3+}}$ was 4.97×10^{-4} mM, $L^{MicroCap}_{Pu^{4+}}$ was 4.07×10^{-6} mM, and $L^{MicroCap}_{U^{4+}} = L^{MicroCap}_{U^{6+}}$ was 9.65×10^{-3} mM.

Of the four types of colloids, intrinsic, mineral, and microbial colloids are assumed filtered or destabilized during transport to the overlying Culebra dolomite strata for PA modeling. Thus, the primary criticality concern of colloidal material is from intrinsic, mineral, and microbial colloids filtered or destabilized.

Information Only

Table VII. Example of Mean and Maximum Total Plutonium and Uranium Concentration in Castile Brine from Dissolved and Four Colloidal Types for CRA-2019 and CRA-2026.

Actinide	Baseline $S^{BaseEQ3/6}_{Ox,Br}$ (mM)	Uncert Factor $10^{f^{D}_{uncrt,Ox}}$	Dissolved $^{uncrt}S^{D}_{Ox,Br}$ (mM)	Colloids: Humic Scale Factor $f^{humic}_{Ox,Br}$	Colloids: Microbe Scale Factor $f^{microbe}_{Ox,r}$	Mineral $C^{mineral}$ (mM)	Intrinsic C^{int}_{r} (mM)	Total Concentration $^{uncrt}C^{T}_{Ox,Br}$ (mM)	Fraction Colloid	Filterable Colloid Fraction (microbe mineral intrinsic)
CRA-2019 [13, Table GEOCHEM-61]										
Castile Brine with Mean Uncertainty Factor										
Pu^{3+}	1.78×10^{-4}	4.48	8.0×10^{-4}	0.20	0.03	2.6×10^{-5}	9.5×10^{-6}	9.3×10^{-4}	0.22	0.07
Pu^{4+} U^{4+}	5.44×10^{-5}	0.97	5.3×10^{-5}	0.01	0.21	2.6×10^{-5}	4.3×10^{-5}	1.3×10^{-4}	0.60	0.60
U^{6+}			1	0.51	0.21	2.6×10^{-5}	1.4×10^{-6}	1.01	0.01	0
				1.1×10^{-2}mM	3.8×10^{-5}mM					
Castile Brine with Maximum Uncertainty Factor										
Pu^{3+}	1.78×10^{-4}	933	1.7×10^{-1}	0.20	0.03	2.6×10^{-5}	9.5×10^{-6}	$^{*}2.0\times10^{-1}$	0.17	0.03
Pu^{4+} U^{4+}	5.44×10^{-5}	27	1.5×10^{-3}	0.01	0.21	2.6×10^{-5}	4.3×10^{-5}	$^{*}1.6\times10^{-3}$	0.08	0.08
U^{6+}			1	0.51	0.21	2.6×10^{-5}	1.4×10^{-6}	$^{*}1.01$	0.01	0.07
CRA-26-19P[Domski, 2025 #3054]										
Castile Brine with Mean Uncertainty Factor										
Pu^{3+}	1.15×10^{-2}	0.32	3.7×10^{-3}	0.40	2.92	2.6×10^{-5}	9.5×10^{-6}	5.2×10^{-3}	0.29	0.75
Pu^{4+}	5.67×10^{-5}	0.17	9.9×10^{-6}	0.01	0.21	2.6×10^{-5}	4.3×10^{-5}	7.9×10^{-5}	0.87	0.88
U^{6+}			3.0×10^{-3}	0.51	0.21	2.6×10^{-5}	1.4×10^{-6}			
Castile Brine with Maximum Uncertainty Factor										
Pu^{3+}	1.15×10^{-2}	3.96	4.6×10^{-2}	0.40	2.92	2.6×10^{-5}	9.5×10^{-6}	$^{*}1.2\times10^{-3}$	0.29	0.01
Pu^{4+} U^{4+}	5.67×10^{-5}	3.39	1.9×10^{-4}	0.01	0.21	2.6×10^{-5}	4.3×10^{-5}	$^{*}2.3\times10^{-4}$	0.14	0.14
U^{6+}			3.0×10^{-3}	0.51	0.21	2.6×10^{-5}	1.4×10^{-6}			
				1.1×10^{-2}mM	4.97×10^{-4}mM					

*Set by maximum cap on humic and microbial colloids $L^{cap}_{Ox,r}$

V.D. Concentration of Colloids

As seen in Fig. 10, the solubility Pu^{+3} is always greater than the solubility of Pu^{+4}. As seen in Table VII, the total concentration of Pu^{+3} with colloids remains greater than the total concentration of Pu^{+4} with colloids, though the difference is muted somewhat. The total concentration of Pu^{+4} near its mean values has the highest contribution from colloids: 60% in CRA-2019 and 87% in CRA-2026. Because the concentrations of Pu^{+3} and Pu^{+4} are orders of magnitude below a critical asymptotic concentration (§IV.I), the total concentration with only a 60% to 87% increase is also not critical.

An aggregation of filtered colloids is also not likely critical since the filterable fraction is usually small. More importantly, filterable mineral and microbial colloids adsorb Pu externally (i.e., on the cell surface); thus, this sorption on mineral and microbial colloids is controlled through equilibrium with the solution concentration. The link between colloidal concentration and equilibrium thermodynamics creates a limit on the concentration of colloidal fissile material that cannot reasonably exceed by many orders of magnitude the dissolved concentration of Pu and, thereby, go critical. Pu adsorbed on colloids would readily de-adsorb from a collection of filtered colloids.

VI. SORPTION OF FISSILE MATERIAL

Concentration of actinides released from waste sites on the surface are typically controlled by sorption at the source.[84-86] Actinide sorption onto TRU waste components in the disposal area is omitted in WIPP PAs. Although omitting sorption in the disposal area is conservative for evaluating releases for comparison to 40 CFR 191, omitting sorption is not conservative as related to the potential for post-closure criticality in the disposal region. However, and as discussed in the following sections, (1) the most prevalent sorptive Fe and MgO substrates are uniformly spread throughout the repository and not concentrated in repository sub-regions, and (2) sorption does not typically produce critical concentrations even in microenvironments.

Information Only

VI.A. General Constraints on Sorption in Repository

The largest potentially sorptive materials for ^{239}Pu or ^{235}U in the disposal area are iron corrosion products (Table III) and hydrated MgO ($Mg(OH)_2$) (Table V). These sorptive materials are uniformly distributed throughout the repository; thus, preferential concentration of fissile material in one area is unlikely. Furthermore, these general constraints preventing criticality in the repository are the same before and after an inadvertent intrusion.

Granted, the waste from each storage/generation site contains a wide variety of potentially sorptive material (Table II), such as soils, waste solidifiers (e.g., bentonite clay), corroded metals, and degraded glass; however, these potentially sorptive waste materials are not concentrated in a few drums. Rather, these sorptive materials are also distributed throughout the repository and preferential concentration of plutonium in one area is unlikely. Similarly, substrates and nutrients for biofilms that might cause fissile concentration are also disseminated throughout the repository.

VI.B. Macroscopic Scale in Repository

The minimum Pu mass for criticality provides a sense of the macroscopic scale in WIPP. Assuming sorption/precipitation around Fe or Fe colloidal aggregation, the minimum ^{239}Pu mass is 3.6 kg for rust in Castile brine after an inadvertent human intrusion (Fig. 6). The 4.0-kg mass in Salado brine prior to intrusion is somewhat larger.[26, Figs. 13&35] For standard waste at maximum 0.325 FME ^{239}Pu (measured as fissile kg mass equivalence –Table I) in 14 drums in TRUPACT-II transport package, requires 155 drums to reach 3.6 kg ^{239}Pu (i.e., many standard containers are required to collect enough fissile Pu). Fewer containers are required for CCOs and POCs: 9.5 CCOs at the maximum 0.380 kg ^{239}Pu per drum and 18 POCs at the maximum 0.2 fissile kg mass equivalent ^{239}Pu per drum. In reality even more containers are required: for example, 36.5 POCs are required in Panel 1, Room 3 with an average 0.140 kg ^{239}Pu/POC (panel and room with highest number of POCs at WIPP).[22, Fig. 5]

VI.C. Sorption Process

The sorption process in geologic media is often expressed as the ratio of mobile material (here, the mobile U and Pu in the brine) and material on the immobile rock (such as corrosion products in the repository or dolomite in the Culebra).[f] The distribution coefficient ($K^D_{r/mat}$) for the sorbate radionuclide r in the Freundlich isotherm model is defined as[67, p. 353]

$$\frac{m_r^{sorbt}}{m_{mat}^{substrt}} = K^D_{r/mat}(C_r^e)^{\lambda} \quad (3)$$

where m_r^{sorbt} is mass of attached sorbate radionuclide r on the solid, $m_{mat}^{substrt}$ is the mass of immobile substrate solid, C_r^e is the equilibrium concentration of the sorbate in the solution, and λ is a number > 0. Usually, a linear isotherm model is used where λ is unity (Table VIII).

Table VIII. Sorbent mass, surface area, and sorption coefficients for iron corrosion products and hydrated magnesium oxide

Sorbent	Surface Area (m^2/g)	RN	Sorption Coefficient (K^D) (mL/g)
Iron corrosion	[a]13.1	An^{3+}	[b]$10^{5.7}$
		An^{4+}	[c]$10^{5.0}$
$Mg(OH)_2$	[d]525	An^{3+}	[e]$10^{5.4}$
		An^{4+}	[f]$10^{3.5}$
Culebra dolomite	[g]0.50	An^{3+}	$10^{-2.3}$<[h]$10^{-1.05}$<$10^{-0.4}$
		An^{4+}	$10^{-3.3}$<[h]10^{0}<10^{1}
		An^{6+}	$10^{-4.8}$<[h]$10^{-2.8}$<$10^{-1.7}$

[a] Magnetite[87]
[b] Iron hydroxychloride[87]
[c] Th in seawater measured on SiO_2, $CaCO_3$ Fe_2O_3 Al_2O_3 and TiO_2[88]
[d] Average of silica gel surface areas measured[89]
[e] Ref[90]
[f] Calculated from Ref[91]
[g] Ref[92, App. C]
[h] CRA-2019

If the WIPP repository is somewhat oxidizing, the initial iron corrosion products of the steel within the WIPP repository may be nanoparticles of amorphous ferrihydrite. The amorphous ferrihydrite (nominally $am-5Fe(III)O_3 \bullet 9H_2O$ though the water content varies) may progress, through dehydration and aggregation, to more crystalline oxides,[93] provided metal cations readily absorbed on ferrihydrite do not block the transformation.[94] If the repository is greatly reduced, an $Fe(II)(OH)_2$ iron hydroxide would form instead.

Hence, potential corrosion products in brine include iron hydroxychloride hibbingite ($Fe(II)_2(OH)_3Cl$), green rust (which is Fe^{2+} and Fe^{3+} cations in layered hydroxide anions (OH^-) with

[f] Herein, sorption refers to the accumulation of material at the interface of another material. Sorption subsumes several different mechanisms (e.g., surface complexation and ion exchange) and is not strictly a surface phenomenon.

Information Only

another anion such as Cl^-—$[Fe(II)_3Fe(III)(OH)_8]\bullet[Cl\bullet n H_2O]$),[95;96] magnetite ($Fe(II)Fe(III)_2O_4$), goethite (α-Fe(III)O(OH)),[96] and lepidocrocite (γ-Fe(III)O(OH)—a polymorph of goethite with different crystal structure). Transformation to hematite ($Fe(III)_2O_3$) can take longer. Because ferrihydrite has an indeterminate formula and hematite is less adsorptive, we assume the iron corrosion product is hibbingite or goethite.

VI.D. Geochemical Constraint on Sorption in Repository

A linear isotherm of Pu^{3+} sorption on hibbingite has a very large $K^D_{rust,Pu}$ of $10^{5.7}$ mL/g rust (Table VIII). Hence, most Pu^{4+} will sorb onto the rust. The mass of hibbingite rust from a CCO container is more than the mass of iron in the CCO (i.e., $m^{substrt}_{hbngt} = 1.77 m_{Fe}$ and m_{Fe}=115 kg—Table II).

Based on the definition of a $K^D_{rust,Pu}$, the sorbed concentration is the ratio of available mass to the volume of available rust. For one CCO containing the maximum of 0.380 kg ^{239}Pu, the sorbed concentration on a corroded CCO is

$$\frac{m^{sorbt}_{Pu^{3+}}}{V^{substrt}_{hbngt}} = \frac{m^{sorbt}_{Pu^{3+}}}{1.77 m_{Fe} / \rho^{density}_{hbngt}(1-\phi_{hbngt})} \quad (4)$$
$$= 0.38 \text{ kg Pu } \rho^{density}_{hbngt}(1-\phi_{hbngt})/(1.77)(115\text{kg CCO})$$
$$= 4.5 \text{ kg/m}^3 < 22.8 \text{ kg/m}^3$$

where $\rho^{density}_{rust}$ is 3040 kg/m^3, ϕ_{rust} is 20%, and 22.8 kg/m^3 is the critical asymptotic concentration for a mixture of goethite and Pu in Castile brine (Fig. 6).[g] The sorbed concentration decreases as the volume considered increases. For the entire repository in CRA-26-19P, the sorbed concentration is 1.2 kg/m^3 < 22.8 kg/m^3 (i.e., (67 200 kg ^{239}Pu) $\rho^{density}_{hbngt}(1-\phi_{hbngt})$/(1.77)(73900 t—Table II).

The sorbed concentration of ^{235}U on rust is even more dilute, since the initial mass of ^{235}U is so small (Table I) and only increases ~1/4th of the 67 200 kg ^{239}Pu over 10^4 years from ^{239}Pu decay while the volume of rust is the same (Table I), and the critical asymptotic limit increases to 90 kg/m^3 (Fig. 10).

A similar situation occurs for sorption on $Mg(OH)_2$. Again, using the CCO container since the mass of cellulose and plastic and thereby, MgO, is small. The MgO per CCO is 28.4 kg, as noted in §IV.F. The hydration of MgO to brucite is

$$MgO + H_2O = Mg(OH)_2 \quad (5)$$

Thus, the mass of brucite ($m_{Mg(OH)_2}$) is m_{MgO}• (58.3 g/mole $Mg(OH)_2$/40.3 g /mole MgO) or 41.4 kg. The corresponding $Mg(OH)_2$ volume of 0.0244 m^3 is based on $\rho^{density}_{Mg(OH)_2}$ of 2400 kg/m^3 and $\phi_{Mg(OH)_2}$ of 30%. Hence, the ratio of ^{239}Pu mass to $Mg(OH)_2$ volume is 17.8 kg/m^3, which is less than the critical asymptotic limit of 90 kg/m^3 for salt-$Mg(OH)_2$ one to one mixture (Fig. 10).

VI.E. Constraint on Sorption in Culebra Dolomite

Criticality is unlikely for ^{239}Pu and ^{235}U sorption on dolomite. Sorption concentration on Culebra dolomite is not critical when bounding sorption by using the solubility of Pu^{3+}, Pu^{4+}/U^{4+}, or U^{6+} inside the repository (Fig. 10) times the corresponding distribution coefficients (Table VIII). For example, the sorbed Pu^{3+} concentration is 0.19 where mean $\bar{K}^D_{Pu^{3+}Culebra}$ is $10^{-1.05}$(Table VIII), $\bar{\phi}^{matrix}_{Culebra}$ is 0.16, $\bar{\rho}^{density}_{Culebra}$ is 2816 kg/m^3 (Table IV), and $\bar{S}^{rep}_{Pu^{3+}}$ is 3.7×10^{-3} mM (Fig. 10):

$$\frac{m^{sorbt}_{Pu^{3+}}}{V^{substrt}_{Culebra}} = K^D_{Pu^{3+}/Culebra} C^e_{Pu^{3+}} [M^{weight}_{Pu} \rho^{density}_{Culebra}(1-\phi_{Culebra})]$$
$$< K^D_{Pu^{3+}/Culebra} \bar{S}^D_{Pu^{3+}} [M^{weight}_{Pu} \rho^{density}_{Culebra}(1-\phi_{Culebra})] \quad (6)$$
$$= 0.19 \text{ kg/m}^3 < 3.7 \text{ kg/m}^3$$

The sorption concentrations of $^{239}Pu^{3+}$ of 0.19 kg/m^3 for $^{239}Pu^{3+}$ and 5.6×10^{-3} kg/m^3 for $^{239}Pu^{4+}$ on Culebra dolomite are less than the critical asymptotic limit of 3.7 kg/m^3 for ^{239}Pu (Fig. 6). Likewise, sorption concentrations of 5.6×10^{-3} kg/m^3 for $^{239}U^{4+}$ and 2.7×10^{-3} kg/m^3 for $^{239}U^{6+}$ on Culebra dolomite are less than critical asymptotic limit of 190 kg/m^3 for ^{235}U (Fig. 7).

Thus, the density of sorption sites on dolomite would have to be very large, especially, since surface complexation at sorption sites would not be limited to ^{239}Pu. The measured mass-specific surface area on carefully crushed and lightly acid-washed samples of dolomite from the WIPP Air Intake Shaft, as evaluated by Brunauer-Emmett-Teller (BET) surface area analysis, varies from 500 m^3/kg to 2600 m^3/kg for Culebra dolomite;[92, App. C] 2600 m^3/kg corresponds to ~3.6×10^6 m^2 surface area per m^3 of dolomite (assuming an available 16% porosity and 2816 kg/m^3 Culebra dolomite grain density).[26, Table II;28, Table II] Thus, the critical Pu concentration of 3.7 kg/m^3 (Fig. 6) corresponds to 2.6 atoms/nm^2 of dolomite surface

[g] As explained when developing Fig. 6 for rust, goethite is used for developing a critical asymptotic limit since hibbingite includes Cl^-, which decreases the reactivity of a mixture of ^{239}Pu, rust, and Castile brine.[26, Fig. 13]

Information Only

which is higher than the observed site density for natural minerals (~2.3 sites/nm^2).[97]

Thus, obtaining a critical concentration requires more than the entire surface capacity of Culebra dolomite. Consequently, sorption, by itself, is an unlikely mechanism for concentrating massive amounts of fissile material in a small area to obtain a critical solid concentration.[h]

VII. PRECIPITATION

VII.A. Constraint on Precipitation in Disposal Area

A uniform distribution of Fe and MgO implies that the geochemistry is fairly uniform without local variation in pH or reduction-oxidation potential to promote preferential precipitation, where the scale is at least 9 CCOs and up to 155 standard drums (as discussed in §VI.B). For example, there is little chance of great variation in the redox state of the brine from one place to another, because Fe^0 iron is present throughout the waste. To elaborate, the main determinant of oxidation states within the repository will be the rate of interaction with elemental iron, Fe^0, and the rate of microbial-facilitated reduction of oxidized species, such as nitrate and sulfate. The resulting repository brines are expected to have relatively high concentrations of reducing species such as Fe^{2+} and S^{2-}. Hence, the most likely states are Pu^{3+} and Pu^{4+} and not higher oxidations states of Pu^{5+} and Pu^{6+}. Surplus non-pit Pu will be disposed as PuO_2 (Pu^{4+}), and reduction of Pu^{4+} to Pu^{3+} would increase the solubility of Pu, not decrease it (Fig. 10).

After any inadvertent human intrusion, gas pressure can be released and allow more brine to enter the repository. Like the situation prior to intrusion, however, a uniform distribution of Fe and MgO implies that the geochemistry is fairly uniform without local variation in pH, ionic strength, or reduction-oxidation potential to promote preferential precipitation.

After an inadvertent human intrusion into a hypothetical pressurized brine source below the repository, much more brine can flow into the repository (mean factor of 2.5 more brine after intrusion into a hypothetical brine source—§VIII.B).[98, Table 4-5] However, the Castile brine in the repository does not substantially change the solubility of the ^{239}Pu either in the +3 or +4 oxidation state (i.e., the solubility is of the same order of magnitude—Fig. 10). Hence, the Castile brine does not introduce a geochemical situation for precipitation within the repository. Rather, the uniform distribution of Fe and MgO still maintains low variability of the pH or reduction-oxidation potential to promote preferential precipitation.

VII.B. Constraints on Precipitation in Culebra: Lack of Favorable Depositional Features

The fissile solution must be greatly concentrated from its repository concentration in CRA-2019 and CRA-2026 to form a critical concentration in the Culebra saturated zone (§IV.I). Yet, like the disposal area, several unfavorable geochemical conditions exist to prevent criticality within the geologic system from precipitation, sorption, and colloidal filtration. The necessary condition for precipitation of fissile material and other major components of the brine is a change in the brine chemistry, which includes the redox state and buffer capacity, pH, ionic strength, or solute concentrations, such that the solubility of a component is reduced.

Change in Redox State. The traditional mechanism of forming uranium ore bodies occurs through precipitation by reduction of a more soluble U^{6+} to less soluble uranium (such as U^{4+}). However, only low concentrations of uranium precipitated. For example, Uranium deposition, as UO_2, often occurred in permeable sandstone. Deposits in Wyoming and the Colorado Plateau, which represent ~30 wt. % of the world`s uranium reserves, are low-grade ores with between 0.1 wt.% and 3 wt.% UO_2. Yet, the minimum asymptotic criticality concentration in Culebra dolomite is 190 kg/m^3 at 20% porosity (Fig. 7), which translates to ~8 wt.%.[26, Fig. 22]

Two hypothetical scenarios of precipitation from oxidation seem unlikely: (a) the oxidation of Pu^{3+} to less soluble Pu^{4+} as it is removed from the Fe^0 in the repository and (b) the oxidation of Fe^{2+} to Fe^{3+}, sorption of Pu on the rust, and coprecipitation with Pu. However, a strong oxidant (or a strong reductant species) in a localized area has not been discovered within the Culebra as regards these hypotheses. Just as important, formations above and below the Culebra also do not have complexing agents such as vanadium or indigenous reductants/oxidants.

[h]In a dual porosity formulation, retardation of Pu in the Culebra strata occurs because of (1) chemical sorption on the fracture flow surfaces (chemical retardation), and (2) diffusion into the pores of the matrix (physical retardation). Physical retardation is the most important mechanism for limiting Pu transport to the land withdrawal boundary (Fig. 1). The Pu diffusing into the brine filled pores does not deposit and fill the pores as occurs with precipitation; rather, the pore fluid concentration approaches the Pu fracture concentration. The post-closure criticality limits of §IV are not noticeably influenced by the small additional amount of Pu dissolved in the matrix pore fluid; none-the-less, the limits reported here (e.g., 3.7 kg/m^3) include dissolved fissile material in the pores and fractures.

Information Only

Furthermore, the availability of sufficient oxygen from the surface through a degraded plug with the permeability of silty sand is unlikely. Consequently, a substantial change in the redox state (Eh) of the brine as it moves through the Culebra is unlikely. Any precipitation or coprecipitation that might occur would be gradual and diffuse over an area too large to cause criticality.

Carbonate Rich Brine. Uranium ores in sedimentary rocks other than sandstone are uncommon in the United States (<5%). Conditions for the deposition of uranium in carbonate rocks, such as limestone or dolomite, are especially unfavorable because carbonate complexes are highly soluble; thus, carbonate rocks typically contain no more than 1 ppm uranium.[99] Plutonium carbonates are also highly soluble. Thus, conditions for deposition of plutonium in the Culebra dolomite are unfavorable.

Granted, uranium is associated with carbonate rocks under some circumstances. For example, a small uranium ore deposit of the Jurassic Period occurs near Grants, New Mexico, the Entrada Sandstone aquifer, overlain by the Todilto Limestone Formation (like dolomite but lacking Mg). A highly fractured area allowed water carrying uranium to move into the limestone and deposit uranium in the presence of H_2S.[2] Another situation occurs in Germany. Three main types of vein deposits occur in the Schlema uranium field of the western Ore Mountains of Germany (the largest vein-style uranium deposit in the world). One vein type consists of uraninite and dolomite formed when uranium in the area was remobilized and deposited under reducing conditions (~170 Ma).

VIII. HYDROLOGIC CONSTRAINTS FROM PA MODELING

VIII.A. Modeling Scenarios

In the PA, the human intrusion scenario was divided into a drilling intrusion through repository to underlying brine reservoir in the Castile Formation (scenario A_{E1}); intrusion into only the repository (scenario A_{E2}), and two intrusions one of which intersects an underlying pressurized brine source (scenario A_{E2E1}). The largest releases to the Culebra occur from the drilling intrusion scenarioA_{E1} and scenario A_{E21}. In scenario A_{E1}, a human exploring for minerals drills through the repository and into a hypothetical underlying brine source. Later, the driller plugs the borehole using concrete (present-day technology) and abandons it. Releases over the long term occur from hypothetical degradation of the concrete seal 200 years later (i.e., borehole permeability set to permeability of sand) and migration of radioisotopes to the Culebra brine saturated zone above the repository (Fig. 11).[i]

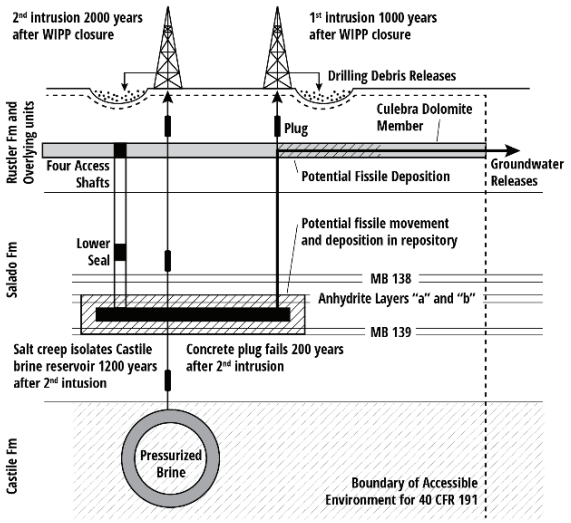

Fig. 11. Hypothetical future release of radionuclides to the Culebra after disruptive human intrusion into repository in Scenario A_{E2E1}.[2, Fig. 2;31, Figure 5.1-2]

In scenario A_{E21}, an inadvertent intrusion into the repository occurs sometime after closure; a second intrusion borehole into repository and Castile brine source occurs later. The concrete plug in the lower portion of second borehole fails 200 years later allowing flow through entire repository and up the first intrusion borehole. In both intrusion scenarios into the Castile brine source, salt creep isolates the Castile brine source 1200 years after the initial intrusion (Table IX).

The three intrusion scenarios were further divided into computational scenarios based on the time of intrusion (Table IX). The largest releases occur from intruding into the repository 100 years after closure. Computational scenarios A_{E1}-BF-t100 and A_{E2E1}-BF-t100 have the potential to release the most Pu and are used here.

[i] Solid, continuous concrete plugs are expected to remain intact for the 10,000-year regulatory period. Only segmented plugs are assumed to degrade. Hence, a probability of failure is associated with the type of plugs used to seal the abandoned borehole, but not used here.

Information Only

Table IX. Designation of Computational Scenarios for Modeling Brine Flow and Repository Radionuclide Transport from Intrusion into the WIPP Repository.[100, Table 5]

ID	Short Description	Description
A_U -BF	Undisturbed or Base Case (A_U)	Predicted behavior of the WIPP disposal system when not disrupted by human intrusion or unlikely natural events
A_{E1}-BF-*t100* A_{E1}-BF-t350	E1 intrusion after 350 and 100 years (computational components of scenario A_{E1})	Inadvertent intrusion into the repository and underlying pressurized brine reservoir in the Castile 350 years after closure; flow up intrusion borehole to Culebra occurs 200 years later when borehole concrete plug fails (i.e., seal permeablity set to sand); salt creep isolates underlying Castile brine source 1200 years after intrusion; for the 100-year intrusion, the 350-y simulation result is linearly shifted to approximate intrusion time at 100 years.
A_{E1}-BF-t1000 A_{E1}-BF-*t2000* A_{E1}-BF-*t4000* A_{E1}-BF-*t6000* A_{E1}-BF-*t9000*	E1 intrusion after 1000, 2000, 4000, 6000, and 9000 years (components of A_{E1})	Inadvertent intrusion into the repository and pressurized brine reservoir in the underlying Castile 1000 years after closure; flow up borehole to Culebra occurs 200 years later when seal fails; salt creep isolates Castile brine source 1200 years after initial intrusion; other intrusion times approximated by linear shifting results at 1000 years to intrusion time of 2000, 4000, 6000, and 9000 years.
A_{E2}-BF-*t100* A_{E2}-BF-t350	E2 intrusion after 350 and 100 years (components of A_{E2})	Inadvertent intrusion into the repository 350 years after closure; radionuclide transport up intrusion borehole occurs 200 years later when concrete plug fails; for the 100-year intrusion, the 350-y simulation result is linearly shifted to approximate intrusion time at 100 years.
A_{E2}-BF-t1000 A_{E2}-BF-*t3000* A_{E2}-BF-*t5000* A_{E2}-BF-*t7000* A_{E2}-BF-*t9000*	E2 intrusion after 1000, 3000, 5000, 7000, and 9000 years (components of A_{E2})	Inadvertent intrusion into the repository 1000 years after closure; radionuclide transport up intrusion borehole occurs 200 years later when concrete seal fails ; other intrusion times approximated by linear shifting results at 1000 years to intrusion time of 2000, 4000, 6000, and 9000 years.
A_{E2E1}-BF-*t100* A_{E2E1}-BF-*t350* A_{E2E1}-BF-t1000 A_{E2E1}-BF-*t2000* A_{E2E1}-BF-*t4000* A_{E2E1}-BF-*t6000* A_{E2E1}-BF-*t9000*	E2 then E1 intrusion after 100, 350, 1000, 2000, 4000, 6000, 9000 years (components of A_{E2E1})	Inadvertent intrusion into the repository occurs 1000 years after closure; 2nd intrusion into repository and underlying Castile brine source occurs 2000 years after closure; seal in lower portion of 2nd borehole fails 200 years later forcing flow through repository panels between second borehole and up 1st intrusion borehole to overlying Culebra dolomite; lower portion of 2nd borehole creeps shut 1200 years after 2nd intrusion; other 2nd intrusion times approximated by linearly shifting results from 2nd intrusion time at 2000 years to 100, 350,1000, 4000, 6000, and 9000 years after closure.

VIII.B. Hydrologic Constraint on Brine Movement Prior to Inadvertent Intrusion

Possible hydrologic mechanisms to move critical masses of the fissile material to more favorable locations within the repository do not exist. Prior to a hypothetical human intrusion, a maximum of 31.8×10^3 m^3 of brine flows *into* the repository through the ubiquitous disturbed rock zone (DRZ) and anhydrite layers in CRA-2019 (Scenario A_U -BF in Table X).

An intrusion somewhat increases the average influx since it can relieve gas pressure (Scenario A_{E2}-BF) but an intrusion into a hypothetical underlying brine source (Scenario A_{E1}-BF or A_{E2E1}-BF) is required to substantially increase brine influx by a factor of 3 or 4 (Table X). Furthermore, an intrusion into a brine source is required to get substantial brine flow up the intrusion borehole and fissile release into the Culebra dolomite.

Table X. Mean cumulative brine flow out of repository and up intrusion borehole in CRA-2019.[101, Table 23]

Location of Brine Flow	Scenario[a]	CRA-2019 Mean[b] (m^3)	Max (m^3)
Into Repository			

Information Only

No Intrusion (into repository)	A_U-BF	-27.0×10^3	-31.8×10^3
Castile Brine Intrusion	A_{E1}-BF	100.0×10^3	250.0×10^3
Repository only Intrusion	A_{E2}-BF	30.6×10^3	37.8×10^3
Repository and Castile Brine Intrusion	A_{E2E1}-BF	60.0×10^3	75.8×10^3
Up Intrusion Borehole			
	A_{E1}-BF	4.72×10^3	7.54×10^3
	A_{E2}-BF	0.096×10^3	0.86×10^3
	A_{E2E1}-BF	4.17×10^3	7.53×10^3

[a]See Table IX
[b]Mean of all 3 replicates (300 samples)

VIII.C. Hydrologic constraints on Deposition in Culebra Dolomite after Inadvertent Intrusion

Because of its higher permeability relative to other strata in the area (other anhydrite layers in the Salado, or layers in the Rustler formation), any dissolved radioisotopes released from the repository through the intrusion borehole enter the Culebra dolomite strata in the sylized simulations. Yet, the probability of criticality is low in the generally inhospitable Culebra. Absent any special circumstance for concentrating fissile material, the general tendency is for fissile material entering the Culebra to disperse because of hydrologic conditions. Hence the most likely area to reach a critical concentration through precipitation, sorption, or colloid aggregation/ filtration of colloids is near the intrusion borehole.

Furthermore, in order to agree with the observed varying salinity in the Culebra saturated zone,[102;103] formations above must slightly recharge the Culebra rather than Culebra fluid leak into other formations in regional groundwater models. Hence, deposition will not tend to occur in adjacent formations.

IX. GEOCHEMICAL CONSTRAINTS IN CULEBRA FROM PA MODELING

IX.A. Fissile Release to Culebra

In addition to the generally unfavorable geochemical conditions for criticality discussed in the previous sections, the results of the CRA-2019 and CRA-2026 analysis confirm that conditions at WIPP are not conducive to criticality. In particular, we have calculated the mean for all three replicates of A_{E2E1}-BF-t100 for CRA-2019. CRA-26-19P, CRA-26-12P, RPPCR-23-19P, and CRA-2019 (Fig. 12). The fissile material reaching the Culebra dolomite strata, using the calculated flow rates and concentrations of fissile material, was generally low in CRA-2019 and the fissile material reaching the Culebra dolomite strata is below the critical mass in CRA-2026 (Fig. 12).

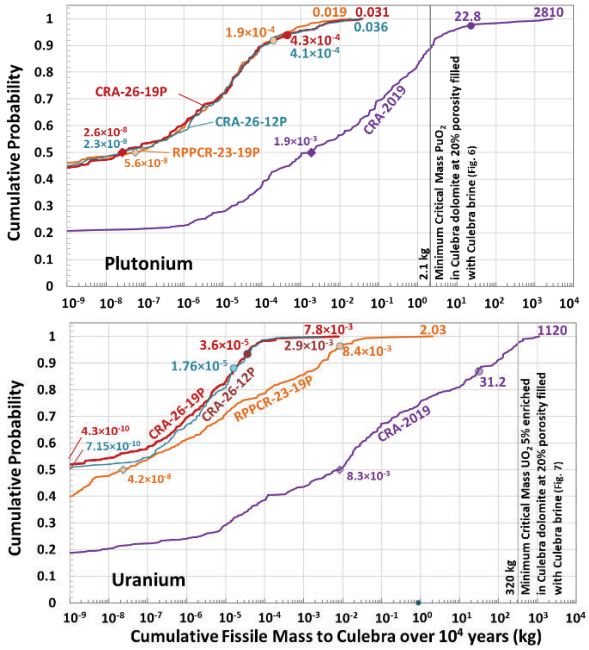

Fig. 12. Distribution of individual ^{239}Pu and ^{235}U cumulative releases to Culebra for computational scenario A_{E2E1}-BF-t100 when all 3 replicates combined for CRA-26-19P, CRA-26-12P, RPPCR-23-19P, and CRA-2019.

The ^{239}Pu releases are approximately lognormally distributed. Hence the largest releases are several orders of magnitude greater than the means. The large uncertainty associated with Pu^{3+} solubility shown in contributes to this difference (Table VII and Fig. 10).

In each replicate, only a few simulations of the A_{E1}-BF-t100 and A_{E2E1}-BF-t100 computational scenarios show extensive Pu releases (Fig. 13). These large Pu releases occur when the uncertainty of Pu^{3+} is near its maximum (e.g., a factor of 933 for CRA-2019). In the first replicate (r1) of CRA-2019, Run 7 (out of 100) had the largest cumulative Pu release (609.74 kg). In r2, Run 68 had the largest Pu release (853.23kg). In r3, Run 66 had the largest Pu release (91.93 kg) (Table IX).

The maximum Pu releases are associated with high brine releases, but not necessarily the largest (Table XI and Fig. 13).

Information Only

Table XI. Mean and maximum cumulative brine and Pu releases to Culebra in A_{E1}-BF-t100 of CRA-2019

		Brine			Pu			
Scenario	**Replicate**	**Mean (m^3)**	**Max (m^3)**	**Max Run**	**Mean (kg)**	**Max (kg)**	**Max Brine (m^3)**	**Max Run**
A_{E1}-BF-t100	r1		152 000	17	9.01	609.74	95 300	7
	r2		75 900	36	14.19	853.23	72 000	68
	r3		129 000	66	1.38	91.93	129 000	66
	Average				8.19			

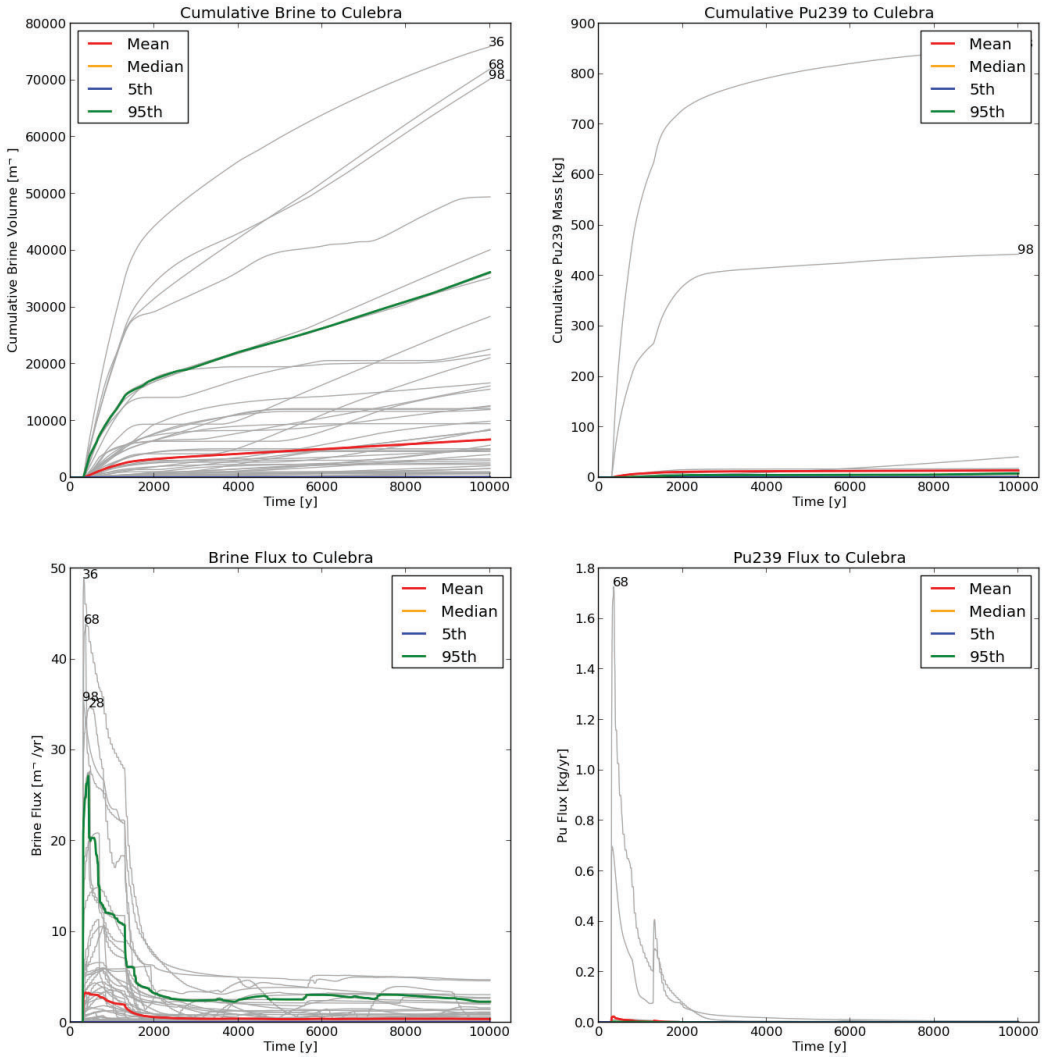

Fig. 13. Cumulative volume and flow rate of brine and cumulative Pu mass and flux into Culebra over 10,000 years from an intrusion that occurs 100 years after closure in Replicate 2 of CRA-2019 (A_{E1}-BF-t100-r2).

Information Only

IX.B. Supplemental Analysis of Pu Dispersion in Culebra

Generally, the CRA-2019 and CRA-2026 performance assessments evaluate radionuclide transport in the Culebra dolomite on a macroscale using MODFLOW and SECOTP. Here, supplemental simulations were made on a microscale for CRA-2019 using PFLOTRAN version 1.01,[104] to provide additional justification to conclusions based on qualitative arguments.[j] Specifically, supplemental simulations evaluated the size of the zone in which dilution and potential precipitation might occur because of changes in ionic strength or pH. The boundary conditions were the same as for regional flow model in CRA-2019, and the regional flow fields from PFLOTRAN are identical to CRA-2019. Here, the supplementary simulation from Run 68 of A_{E1}-BF-t100-r2 is used, because of the large Pu solubility and, thereby, large Pu releases. The maximum cumulative brine flow to the Culebra is 72 000 m^3 over 10^4 years (Table XI). This large brine flux causes a major perturbation in the Culebra flow field. The second supplementary simulation used the mean brine flux from all 100 runs of A_{E1}-BF-t100-2r (7000 m^3 cumulative brine value, which is more than an order of magnitude less) to evaluate a situation with much less perturbation of the Culebra flow field.

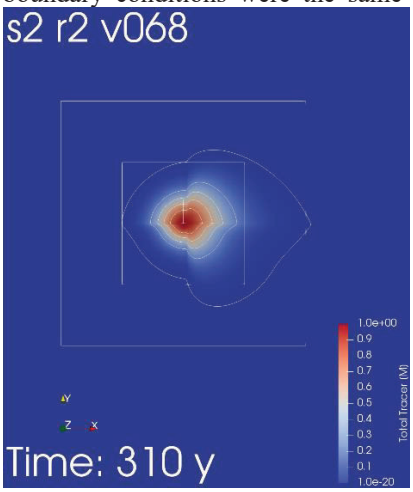

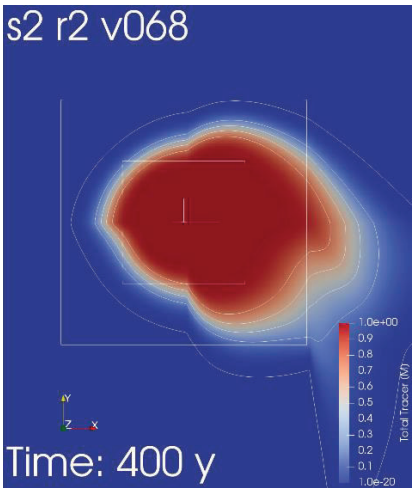

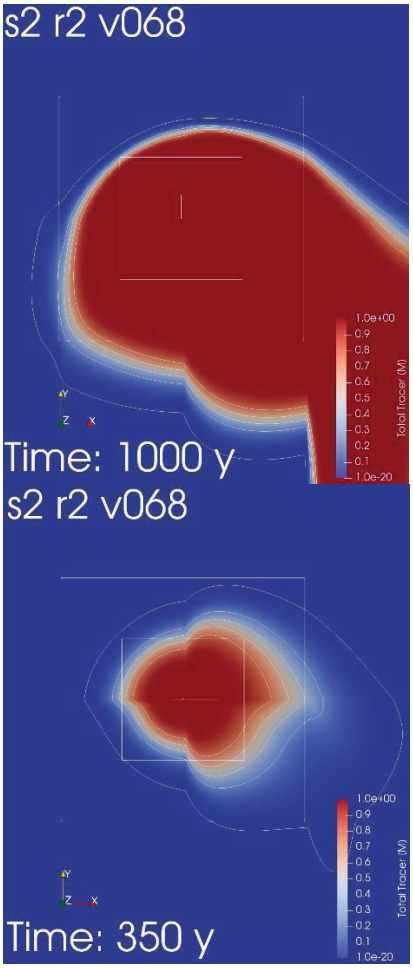

[j] PFLOTRAN will replace MODFLOW and SECOTP in the future. The PFLOTRAN capabilities used here were qualified for the CRA-2019 application.[105]

Information Only

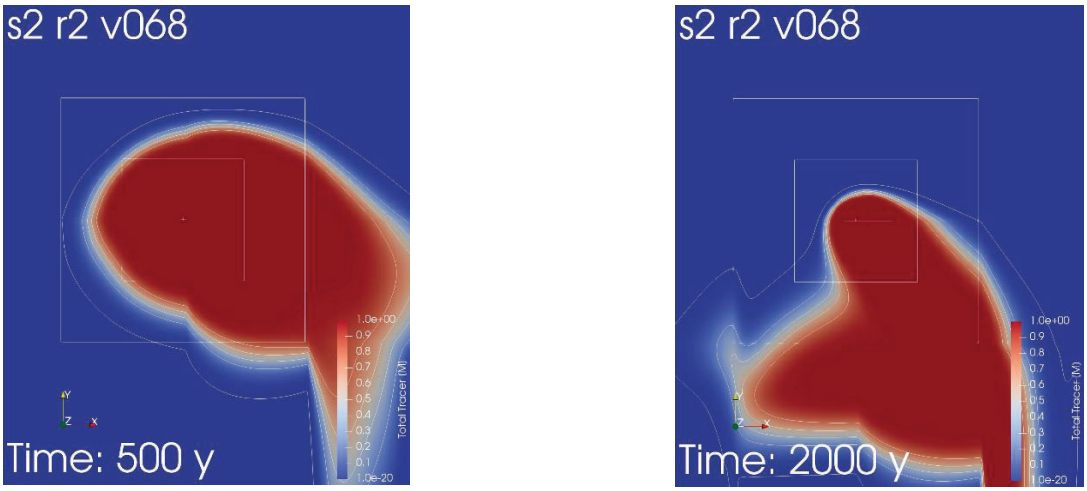

Fig. 14. Plume of non-adsorbing tracer in Culebra at intrusion borehole between 310 years and 2000 years with brine flux of 72 000 m^3 in run 68 of computational scenario A_{E1}-BF-t100-r2; lines at borehole are 5 m, 10 m, and 15 m long; boxes are 50 m and 100 m on a side; contours are at normalized tracer release of 0.001, 0.2, 0.4, 0.6, and 0.8.

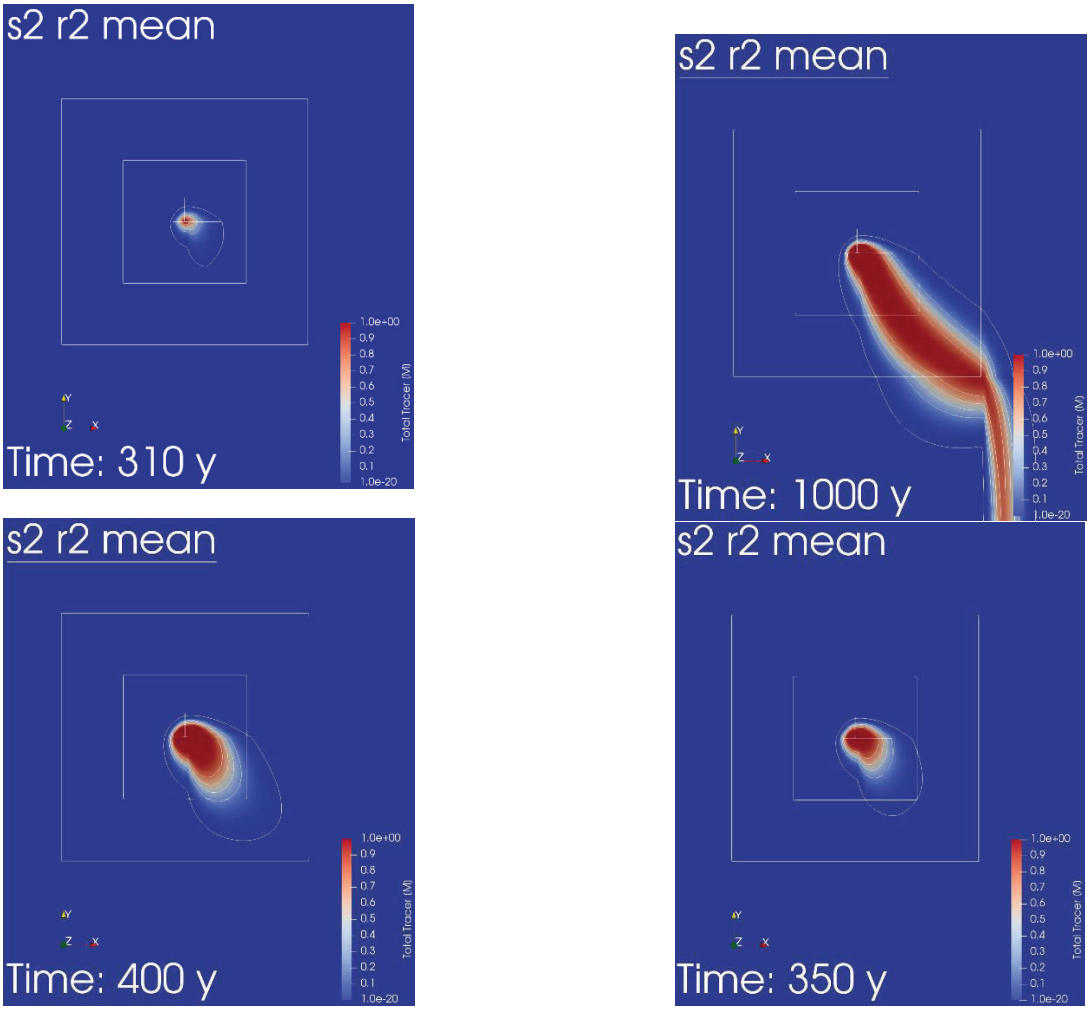

Information Only

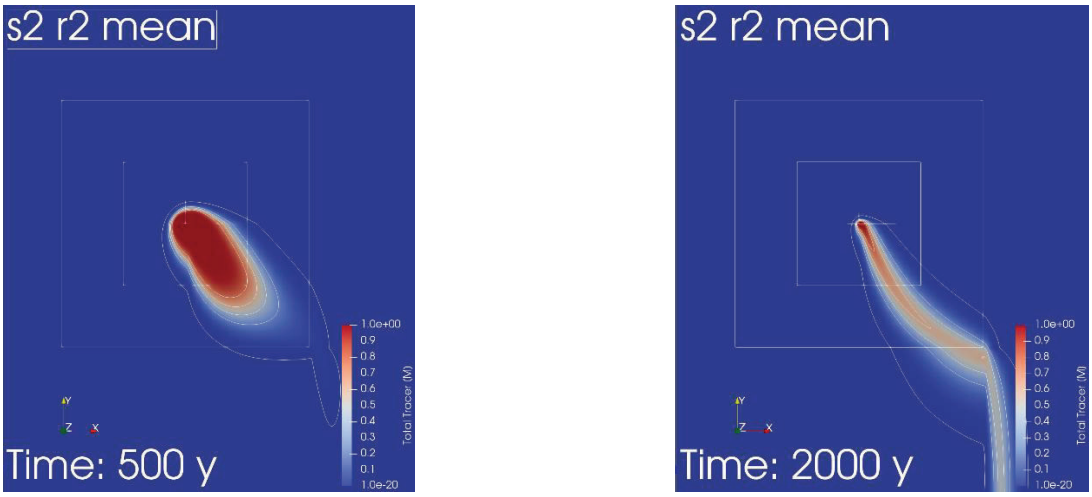

Fig. 15. Plume of non-adsorbing tracer in Culebra at intrusion borehole between 310 years (10 years after plug to Castile brine source fails in 100-year intrusion) and 2000 years (800 years after salt creep closes off Castile brine source) with mean brine flux of all 100 runs of scenario A_{E1}-BF-t100-r2.

In WIPP PAs, the uncertainty in fluid flow is represented by 100 Culebra flow fields generated from 100 conditioned transmissivity fields (PEST/MODFLOW). In these 100 flow fields, the uncertainty in fluid flow directly above the disposal waste panels, as represented by the standard deviation of the Darcy velocity, is small (Fig. 16).

Information Only

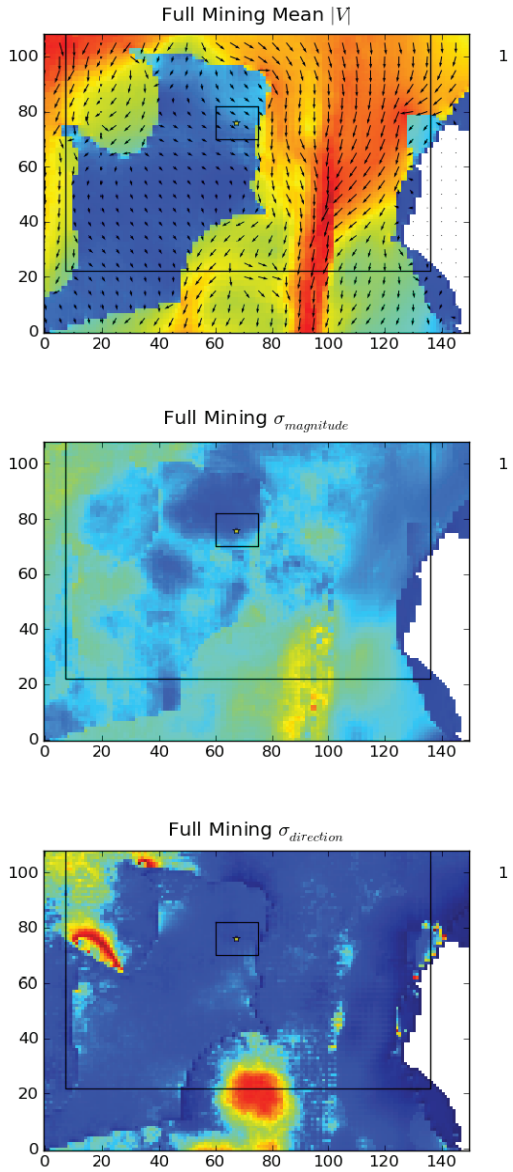

Fig. 16. Average Darcy velocity between 10.5 and 9.0 m/s, standard deviation between 0 and 0.6 m/s, and directional standard deviation between 0 and 0.3 of $\tan^{-1}(v_y/v_x)$ above WIPP panels (small black rectangle) for 300 flow fields of scenario where potash mining disrupts the Culebra flow field. The large rectangle is the land withdrawal boundary.[106, Figure 4-3]

The Darcy velocity variability is small because several well measurements above the near the repository constrain the variability. The microscale of our calculations is about 100 m and thus within the 629-m by 776-m boundary of the disposal panels (Fig. 1). Consequently, it does not matter which flow field is chosen for our calculations. We chose the first flow field generated.

IX.C. Lack of Conditions for Precipitation in Culebra

Change in Ionic Strength. As WIPP repository brine enters and mixes with Culebra brine, the ionic strength will drop from between 6700 and 5300 mM to 800 mM (Table II). Many minerals have a higher solubility in high ionic strength brines than in low salinity solutions. Hence, as the brine from the repository is diluted in the Culebra dolomite strata, the solubility could decrease. A possible situation is the dilution of Pu^{3+} in a Castile-dominated brine to a Culebra-dominated brine.

Change in pH. The pH and CO_2 concentration in the repository is controlled by the addition of excess MgO to form brucite, $Mg(OH)_2$, at a buffered pH of 9. Contaminated brines entering the Culebra will carry dissolved $Mg(OH)_2$, but little solid MgO, so the pH could drop from alkaline to near neutral of the Culebra brine (Table II), and the CO_2 concentration rise, as the $Mg(OH)_2$ was consumed by the Culebra CO_2 to form hydromagnesite $Mg_5(CO_3)_4(OH)_2\bullet H_2O$. The change in pH and CO_2 concentration could cause co-precipitation of plutonium or uranium carbonates within the Culebra pore space; however, changes in pH and availability of CO_2 would still be dependent on sufficient mixing of the two brines.

Modeling brine mixing. The large perturbation of the Culebra flow field by the injection of ~72 000 m^3 of Castile brine at the intrusion borehole results in an initially large mixing zone for the largest release (run 68 of A_{E1}-BF-t100-r2). Based on the normalized concentration contours between 0.2 and 0.8 of a non-adsorbing tracer, the mixing zone is ~1180 m^2 in the first 10 years assuming a circular annulus with a minimum radius of 5 m and maximum of 20 m (Fig. 14).

Although the annulus width of the mixing zone decreases at later times, the diameter keeps increasing such that the mixing zone area increases by a factor of 1.5 (1810 m^2 with 8 m annulus at 32 m radius—Table XII). If one uses the Pu flux rate of run 68 of A_{E1}-BF-t100-r2 (Fig. 13), a rough estimate of the concentration in the mixing zone is possible. Although the 294 kg Pu mass released between 500 and 1000 years of CRA-2019 is large, the volume is so large (even when assuming deposition in only one meter of the 4-m thick Culebra) that the Pu concentration of 0.25 kg/m^3 (Table XII) remains a factor of 15 below the critical concentration of 3.7 kg/m^3 (i.e., the mixing volume must be a factor of 15 smaller at a 1000 years).

Information Only

Table XII. Mixing zone and corresponding Pu concentration for E1 intrusion at 100 years and Castile plug failure 200 years later in CRA-2019 (Scenario A_{E1}-BF-t100-r2)

Time since WIPP Closure (y)	Time since Castile Plug Failed (y)	Cumulative Pu Released in CRA-2019 (kg)	Pu Flux	Mixing Radius to 0.8 contour (m)	Annulus to 0.2 contour (m)	Volume[a] (m^2)	Pu Conc (kg/m^3)
Area of mixing of ~72 000 m^3 brine flow (cumulative) of Scenario S2-BF-t100-r2 for run 68 (Fig. 15)							
310	10	11		5	15	1180	0.001
350	50	76	65[b]	23	9	1560	0.04
400[c]	100	151	75	32	8	1810	0.04
500	200	256	105	35	7	1690	0.06
1000	700	550	294	35	5	1180	0.25
Mixing area for mean brine flow (7000 m^3 total) and 8.2-kg mean Pu release in S2-BF-t100-r2 (Fig. 16)							
310	10	2.23		1	3	47	0.047
350[d]	50	8.2[e]		5	3	123	0.067

[a]Volume assumes 1 m flow thickness in 4-m thick transmissive Culebra dolomite
[b]Because the mixing zone changes location, only the difference between successive time steps is used (e.g., 310 and 350 years); however, even assuming the entire mass released was in the mixing zone would not cause criticality.
[c]Mixing area remains fairly circular through 400 years because of the large brine flux from the borehole
[d]Mixing area transitions to a more traditional elliptical shape after 350 years
[e]8.2 kg is cumulated over 10 000 years (Fig. 12)

The mean brine flux rate perturbs the Culebra regional flow field much less, and the zone of mixing is between 47 m^2 and 123 m^2 in the first 10 and 50 years, respectively (Fig. 15). However, the Pu concentration remains orders of magnitude below the critical concentration (i.e., Pu concentration between 0.047 and 0.067 kg/m^3 < 3.7 kg/m^3 critical concentration) (Table XII).

Although an exhaustive search of the probabilistic combinations to find a situation of a minimum flow field disturbance and maximum Pu discharge could be conducted, the order of magnitude variation in brine flow simulated here spans the range of behavior. Over this range of behavior, the Pu concentration remains orders of magnitude below the critical concentration of 3.7 kg/m^3. Consequently, the simulations suggest chemistry changes from mixing will likely occur over a wide area as the brine flux up the borehole varies with time.

IX.D. Lack of Conditions for Sorption in Culebra

While precipitation would occur in the mixing zone between the Salado/Castile brine and Culebra brine as the brine chemistry changed, sorption would tend to occur next to the borehole. These two zones do not overlap except during the initial Pu release. By 10 years, the zones have diverged. For the Pu^{3+} discharge of 188 kg at 10 years in Scenario A_{E1}-BF-t100-r1 of CRA-2019 (Table XII), the maximum cylinder radius is 2.2 m to reach a critical concentration of 12 kg/m^3 in Salado or Castile brine, which would be the dominate fluid at the borehole (or 4.5 m to reach a critical concentration of 3.7 kg/m^3 in Culebra brine—Fig. 6) assuming deposition in one meter of the 4-m thick Culebra. In comparison, the radial distance to the mixing zone is already 5 m at 10 years when the cumulative brine discharge is 72,500 m^3. Similarly, the maximum cylinder radius is 0.24 m in Castile brine (or 0.5 m in Culebra brine) for the mean Pu^{3+} release of 2.23 kg at 10 years. In comparison, the radial distance to the mixing zone at 10 years is 5 m when the cumulative brine discharge is 7000 m^3 (Table XII).

Information Only

X. Summary: Rationale for Hydrologic and Geochemical Constraints on Criticality in WIPP Disposal System

Hydrologic and geochemical processes cannot sufficiently concentrate fissile material (consisting primarily of ^{239}Pu but also ^{235}U) to cause criticality in and around WIPP, based on the qualitative low-probability rationale, presented here. This situation is true even when considering the disposal of surplus Pu TRU waste in POCs and CCOs.

Herein, the probability of criticality is notionally conceived as the sum of the low probability of fluid flow, dissolution, precipitation, sorption, and colloidal aggregation sufficiently concentrating fissile material in the repository and geologic barrier prior to and after disruption of the WIPP disposal system by inadvertent human intrusion.

X.A. Constraints within Repository Prior to Hypothetical Human Disruption

After extensive container degradation but prior to inadvertent intrusion by exploratory drilling into WIPP, hydrologic conditions constrain the location, sufficiency of brine, and contribution to mixing. Specifically, brine from the host salt seeps into the repository rather than out, preventing deposition of fissile ^{239}Pu and ^{235}U in adjacent geologic strata. In some simulations, brine seepage is completely consumed by anoxic corrosion of steel containers, in which case, no gradient exists to move fissile material. For those hypothetical situations with large brine inflow, a small 1% dip of the Salado host bedded salt contribute to more uniform mixing of high concentrations of fissile material disposed in northern panels (such as POCs in Panels 1 and 2, and non-pit Pu possibly disposed in Panel 10—Fig. 5) with lower concentrations in southern panels of the repository (Table XIII).

An important constraint on geochemical conditions within the WIPP repository is the uniform distribution of iron in the containers and magnesium oxide (MgO) added in the repository, which keeps the brine chemistry fairly uniform such that pH, ionic strength, and reduction-oxidation potential do not vary widely. To elaborate, MgO reacts with carbon dioxide produced from microbial degradation of organic material in TRU waste and keeps the pH uniformly mildly basic at ~9. In turn, the dissolved concentration of Pu^{3+} or Pu^{4+} remains 3 to 5 orders of magnitude less than the critical limit in Castile brine (Table XIII). Also, the presence of reductants, sorptive material, and colloid substrates, such as ubiquitous iron from waste containers, is well distributed throughout the repository on a macroscopic scale.

An important macroscopic scale in the repository is defined by the minimum critical mass of ~3.6 kg, requires at least 9 CCO, 18 POCs, or 155 standard drums. Molecular diffusion can maintain fairly uniform conditions over these and large scales. Consequently, macroscopic conditions do not promote preferential deposition of sufficient quantities of Pu from between 9 and 155 drums at only one or a few locations (Table XIII).

X.B. Constraints within Repository After Hypothetical Human Disruption

After human intrusion, brine flow may move fissile material within the repository. However, the addition of copious amounts of Castile brine from a hypothetical brine source below the WIPP does not substantially change pH, ionic strength, or the reduction-oxidation potential within the repository and promote sufficient precipitation, sorption or colloidal aggregation to cause criticality.

X.C. Constraints in Culebra After Hypothetical Human Disruption

Hydrologic conditions constrain the deposition location of fissile material released through an intrusion borehole. The relatively greater permeability favors movement of fissile material to the Culebra dolomite above the repository rather than to other strata. Furthermore, fluids tend to flow into rather than out of Culebra; thus, little likelihood exists for deposition in adjacent strata. The dispersion that normally occurs while contaminants move through the Culebra and the lack of known deposition zones suggests that the fissile material brought to the Culebra can only reach a critical concentration near the intrusion borehole. Yet, the typically low solubility of the fissile material implies that vast amounts of brine are required to transport enough fissile material to cause criticality. The large amount and variability of the brine flux spreads out the mixing between the brine from the intrusion borehole and the brine in the Culebra. The subsequently large mixing zone is such that a concentration of 100% enriched ^{239}Pu greater than a criticality limit of 3.7 kg/m^3 cannot be reached (Fig. 6 and Table XIII) (or a concentration of 5% enriched ^{235}U greater than a critical concentration limit of 190 kg/m^3—Fig. 7).

Like the underground facility, several unfavorable geochemical conditions exist to prevent criticality within the Culebra. Uranium ore deposits in evaporates such as the Culebra dolomite are rare because carbonate in the formations increases rather than decreases solubility. Hence, a strong reducing agent is necessary to reduce U^{6+} to U^{4+}. Because a strong reductant (or oxidant) in a localized area has not been discovered within the Culebra, a sudden change

Information Only

in the reduction-oxidation potential is unlikely. More importantly, the 190 kg/m^3 (~8 wt.%) critical concentration required for 5% enriched UO_2 in Culebra dolomite greatly exceeds concentrations found in economically mineable ores (0.1 to 3 wt.% in sandstone).

The solubility of Pu^{4+} in PuO_2 increases with the carbonate abundantly available in the Culebra dolomite brine saturated zone. Granted, the solubility of Pu^{3+} may decrease in the Culebra dolomite brine. However, the large mixing zone within the Culebra mitigates any tendency to precipitate Pu^{3+} in high concentrations. Precipitation would be gradual and diffuse over a large area. Any Pu deposition that occurred would have to at least exceed a low-grade ore concentration (i.e., 2.5 kg/m^3 for 1 wt. % low-grade ore at 1000 ppm) to reach a 3.7 kg/m^3 critical concentration.

Sorption is not a likely mechanism to form critical concentrations of ^{239}Pu and ^{235}U. The possibility of criticality from sorption on Fe or hydrated MgO (i.e., brucite or $Mg(OH)_2$) does not reach critical concentration limits, based on definition of the distribution coefficient (K^D) as the ratio of potential fissile mass in drum, room, panel, or repository and the volume of sorptive Fe or $Mg(OH)_2$.The entire sorption capacity of dolomite is required to reach a critical concentration of 3.7 kg/m^3 for Pu; yet sorption is not exclusive to Pu. Furthermore, sorption and precipitation are not necessarily co-located since sorption would more likely occur at the borehole while precipitation would be at the mixing front.

Regarding colloidal concentrations, the total concentration of Pu^{+4} near its mean values has the highest contribution from colloids: 60% in CRA-2019 and 87% in CRA-26-19P. Because dissolved concentrations of Pu^{+3} and Pu^{+4} are orders of magnitude below a critical asymptotic concentration (§IV.I), the total concentration with only a 60% to 87% increase is also not critical.

An aggregation of filtered colloids is also not likely critical since the filterable fraction is usually small. More importantly, filterable mineral and microbial colloids sorb fissile material externally (i.e., on the cell surface); thus, this sorption on mineral and microbial colloids is controlled through equilibrium with the solution concentration. The link between colloidal concentration and equilibrium thermodynamics creates a limit on the concentration of colloidal fissile material that cannot reasonably exceed by many orders of magnitude the dissolved concentration of fissile material and, thereby, go critical. Fissile material sorbed on colloids would readily de-sorb from a collection of filtered colloids. Finally, colloidal filtration/aggregation of rust colloids, a likely colloidal mineral substrate for fissile material, not critical since sorption on homogeneous mixture of rust not critical.

Although the fore mentioned common conditions for precipitation, sorption, and colloid destabilization/filter in the Culebra dolomite prevent fissile deposition at critical concentrations, this general rationale benefits from arguments more directly tied to the PA analysis. The volume of brine reaching the Culebra dolomite is one example. The transport of fissile material to the Culebra dolomite strata above the repository is another example. The mean and maximum ^{239}Pu release to the Culebra dolomite strata was 2.4×10^{-3} kg and 100 kg in the 1996 CCA; 22.8 kg and 2810 kg in CRA-2019, and 4.3×10^{-4} kg and 3.1×10^{-2} kg in CRA-26-19P (Fig. 12). The large increase from the 1996 CCA and CRA-2019 is because of assumptions on actinide solubility (Fig. 5). However, the large volume of brine required to move the ^{239}Pu in CRA-2019 and its wide variation over the 10^4-y compliance period has a direct influence on the large size of the mixing zone and potential fissile concentration which precludes criticality. The decrease in fissile material release in RPPCR-23 and CRA-2026 is because of the increase understanding of creep closure of an inadvertent intrusion borehole into the repository. The 5-order magnitude decrease in maximum fissile material mass eliminates the possibility of criticality in the Culebra dolomite strata.

Information Only

Table XIII. Rationale for Low Probability of Criticality from hydrologic and geochemistry processes in WIPP Disposal System

Feature ***Event*** **Process**	**Rationale for Hydrologic/Geochemistry Not Causing Criticality**
Room ***Undisturbed*** **Fluid Flow**	**Hydrologic Constraint on Depositional Location in Repository for Undisturbed Condition** 1. Without intrusion, short-term gradient causes brine seepage *into* disposal rooms. 2. In some simulations, brine seepage is completely consumed by anoxic corrosion of steel containers, in which case, no gradient exists to move fissile material
Dissolution	**Geochemical Constraint on Dissolved Concentration in Brine** The asymptotic criticality concentration limit of 30.2 kg/m^3 for ^{239}Pu in Castile brine (Fig. 6) corresponds to 130 mM, a concentration 5 orders of magnitude greater than Pu^{3+} dissolved concentration of 3.7×10^{-3} mM in Castile brine in recent analysis and 2 orders of magnitude greater than the maximum Pu^{3+} solubility ever used in WIPP analysis (Fig. 10); Also, the asymptotic criticality concentration limit of 1550 kg/m^3 for ^{235}U in Castile brine (Fig. 7), corresponds to 6.6×10^3 mM, a concentration almost 4 orders of magnitude greater than the maximum $^{235}U^{6+}$ concentration of 1 mM ever used in WIPP analysis (Fig. 10).
Precipitation	**Geochemical Constraint on Precipitation Concentration** Reducing agents, such as iron (Fe^0) from containers, and MgO added in disposal rooms are well distributed, on macroscopic scale, throughout waste and repository, which keeps brine chemistry fairly uniform; thus, no localized preference for precipitation exists. For example, magnesium oxide (MgO) reacts with carbon dioxide (CO_2) and thereby keeps pH uniformly basic at ~9. Furthermore, reduction of disposed Pu^{4+} as PuO_2 to Pu^{3+} increases Pu solubility.
Sorption	**Geochemical Constraint on Sorption Concentration** 1. Sorptive materials with large mass, such as rust and hydrated MgO (i.e., $Mg(OH)_2$), are well distributed throughout rooms, panels, and repository 2. Sorption concentration on iron rust less than 24.8 kg/m^3 in Salado brine) for Pu^{4+} solubility with corresponding distribution coefficient (e.g., $K^D_{Pu^{4+}/Culebra} S^D_{Pu^{4+}}$) 3. Based on definition of $K^D_{Pu^{3+}/Culebra}$, ratio of maximum $^{239}Pu^{3+}$ mass in CCO to volume of Fe in CCO container or volume of $Mg(OH)_2$ around CCO container < 22.8 kg/m^3. 4. Ratio of total maximum $^{239}Pu^{3+}$ mass to Fe or $Mg(OH)_2$ volume in panel or repository also <24.8 kg/m^3.
Colloid Filtration/ Aggregation	**Geochemical Constraint on Colloid Aggregation Concentration** 1. Substrates for colloid formation well distributed throughout repository; gravitational settling following destabilization of mobile colloids does not cause large colloid aggregation (like dust settling in a closed room). 2. Like dissolved concentrations, the total concentrations with colloids are orders of magnitude below a critical concentration because the colloidal fraction is not greater than one. 3. Colloidal filtration/aggregation of rust colloids, a likely colloidal mineral substrate for fissile material, not critical since sorption on homogeneous mixture of rust not critical.
Repository ***Intrusion*** **Precipitation**	**Geochemical Constraint on Precipitation Concentration in Repository after Intrusion** 1. Fe^0 reducing agent from drums and added MgO well distributed throughout waste and repository, like situation prior to intrusion 2. Addition of Castile brine does not substantially alter the solubility of either Pu^{3+} and Pu^{4+} or U^{4+} and U^{6+}
Sorption	**Geochemical Constraint on Sorption Concentration** Like situation prior to intrusion except critical concentration drops slightly to 22.8 kg/m^3 from 24.8 kg/m^3.
Colloid Filtration/ Aggregation	**Geochemical Constraint on Colloid Filtration Concentration** 1. Although brine flow can stir up colloids, aggregation of suspended colloids would be localized to microenvironments. These microenvironments would be well distributed on a macroscopic scale throughout repository 2. Thermodynamic equilibrium of the dissolved concentration with colloids limits the ability of colloids to exceed the solution concentration by many orders of magnitude.

Information Only

Feature *Event* Process	Rationale for Hydrologic/Geochemistry Not Causing Criticality
Culebra ***Intrusion*** **Fluid Flow**	**Hydrologic Constraint on Deposition Location in Culebra after Intrusion** 1. Relatively greater permeability to other strata favors deposition in Culebra dolomite strata 2. Fluid tends to flow into Culebra dolomite strata rather than out; thus, no deposition in adjacent strata 3. Low solubility of ^{239}Pu and ^{235}U fissile material requires vast amounts of brine; thus, mixing zone of Castile brine carrying fissile material into Culebra dolomite too large to reach 3.7 kg/m^3 Pu critical concentration or 190 kg/m^3 U critical concentration 4. For CRA-2019 with large brine flow, variability in brine flux up the borehole spreads out mixing zone in Culebra dolomite strata. Although solubility of Pu^{3+} decreases in Culebra dolomite when repository brines mix with Culebra brine, hydraulic constraint of moving mixing zone reduces tendency to precipitate Pu^{3+} in high concentrations.
Precipitation	**Geochemical Constraint on Precipitation Concentration in Culebra after Intrusion** 1. U ore deposits in evaporates, such as dolomite, are rare because carbonate in the formations increases rather than decreases solubility 2. At 5% enrichment, 190 kg/m^3 (8 wt.%) critical concentration for UO_2 in Culebra dolomite far exceeds concentrations found in economically mineable ores in sandstone (0.1 wt.% to 3 wt.%) 3. Solubility of Pu^{4+} increases with the carbonate abundantly available in the Culebra dolomite brine; hence, reducing agent is necessary 4. No strong reductants (or oxidants) known in Culebra 5. 3.7 kg/m^3 critical concentration in Culebra dolomite and Culebra brine for Pu^{3+} or Pu^{4+} requires concentrations exceeding low-grade ores (i.e., 2.4 kg/m^3 for 1 wt.% low-grade ore)
Sorption	**Geochemical Constraint on Sorption Concentration** 1. Sorption concentration on Culebra dolomite is not critical for Pu^{3+}, Pu^{4+}, U^{4+}, or U^{6+} concentration when bounded by the solubility in repository with distribution coefficients in the Culebra dolomite (e.g., $K^D_{Pu^{3+}Culebra} S^D_{Pu^{3+}}$). 2. Critical concentration of 3.7 kg/m^3 in Culebra dolomite with Culebra brine (or 8 kg/m^3 with more likely Castile brine) exceeds adsorptive capacity of Culebra dolomite 3. Sorption and precipitation likely occur in different areas of Culebra dolomite (i.e., not collocated); sorption tends to occur next to borehole, while precipitation occurs away from borehole in mixing zone between Culebra and repository brines
Colloid Destabilization/ Filtration	**Geochemical Constraints on Colloidal Destabilization/Filtration Concentration** Colloidal destabilization occurs primarily because of changes in ionic strength which occur over large brine mixing zone too large to cause criticality (like precipitation)

Information Only

REFERENCES

[1] R.P. Rechard, L.C. Sanchez, C.T. Stockman, and H.R. Trellue. 2000. Consideration of nuclear criticality when disposing of transuranic waste at the Waste Isolation Pilot Plant, SAND99-2898. Albuquerque, NM: Sandia National Laboratories.

[2] R.P. Rechard, L.C. Sanchez, H.R. Trellue, and C.T. Stockman. 2001. Unfavorable conditions for nuclear criticality following disposal of transuranic waste at the Waste Isolation Pilot Plant. *Nuclear Technology,* **136** (1) 99–129.

[3] Pub. L. 102-579. 1992. *Waste Isolation Pilot Plant Land Withdrawal Act*, 106 Stat. 4777.

[4] EPA (US Environmental Protection Agency). 1996. 40 CFR Part 194: Criteria for the certification and re-certification of the Waste Isolation Pilot Plant's compliance with the 40 CFR Part 191 disposal regulations; final rule. *Federal Register,* **61** (28) 5224–5245.

[5] R.P. Rechard. 2000. Historical background on performance assessment for the Waste Isolation Pilot Plant. *Reliability Engineering and System Safety,* **69** (1-3) 5–46.

[6] EPA (US Environmental Protection Agency). 1985. 40 CFR Part 191: Environmental standards for the management and disposal of spent nuclear fuel, high-level and transuranic radioactive wastes: final rule. *Federal Register,* **50** (182) No. 182, 38066–38089.

[7] EPA (US Environmental Protection Agency). 1993. 40 CFR Part 191: Environmental radiation protection standards for the management and disposal of spent nuclear fuel, high-level and transuranic radioactive wastes, final rule. *Federal Register,* **58** (242) 66398–66416.

[8] EPA (US Environmental Protection Agency). 2022. Technical support document for sections 193.23, 194.34, and 194.54: review of changes to WIPP performance assessment features, events, and processes in 2019 CRA, Docket: EPA-HQ-QAR-2019-0534. Washington, DC: US Environmental Protection Agency.

[9] M.G. Marietta, D.R. Anderson, G. Basabilvazo, J.C. Helton, and H.-N. Jow. 2000. Summary discussion of the 1996 performance assessment for the Waste Isolation Pilot Plant. *Reliability Engineering and System Safety,* **69** (1-3) 437–452.

[10] DOE (US Department of Energy). 1996. Title 40 CFR Part 191: Compliance certification application for the Waste Isolation Pilot Plant, DOE/CAO-1996-2184. Vol. I-XXI. Carlsbad, NM: DOE Carlsbad Area Office.

[11] R.P. Rechard. 2015. Probability and consequences of nuclear criticality at a geologic repository--I: conceptual overview for screening. *Nuclear Technology,* **190** (2) 97–126.

[12] DOE (US Department of Energy). 2022. Transuranic waste acceptance criteria for the Waste Isolation Pilot Plant, DOE/WIPP-02-3122, Revision 11. Carlsbad, NM: US Department of Energy, Carlsbad Field Office.

[13] DOE (US Department of Energy). 2019. Title 40 CFR Part 191 Compliance Recertification Application for the Waste Isolation Pilot Plant, DOE/WIPP-10-3609. Carlsbad, NM: Carlsbad Area Office, US Department of Energy.

[14] S. Brunell, J. Bethune, P. Docherty, D.C. Kicker, S. Kim, S. King, J. Long, and T.R. Zeitler. 2023. Summary report for the 2023 replacement panels planned change request performance assessment, ERMS 579729. Carlsbad, NM: Sandia National Laboratories.

[15] EPA (US Environmental Protection Agency). 2025. EPA review of DOE replacement panels planned change request, Part 1: Review of DOE 12-panel sensitivity study, Washington, DC: US Environmental Protection Agency, Office of Radiation and Indoor Air.

[16] DOE (US Department of Energy). 2024. Notice of availability of final environmental impact statement for surplus plutonium disposition program. *Federal Register,* **89** (13) 3642–3644.

[17] NA/NRC (National Academies/National Research Council). 2020. Review of the Department of Energy's plans for disposal of surplus plutonium in the Waste Isolation Pilot Plant, Washington, DC: The National Academies Press.

[18] T.R. Zeitler, J. Bethune, S. Brunell, P. Docherty, S. Kim, S. King, and J. Wilgus. 2025. Analysis report for 12-panel PA sensitivity study, Carlsbad, NM: Sandia National Laboratories.

[19] NRC (US Nuclear Regulatory Commission). 2003. Yucca Mountain review plan, final report, NUREG-1804, REV 2. Washington, DC: Office of Nuclear Material Safety and Safeguards, US Nuclear Regulatory Commission.

[20] R.P. Rechard, G.A. Freeze, and F.V. Perry. 2014. Hazards and scenarios examined for the Yucca Mountain disposal system for spent nuclear fuel and high-level radioactive waste. *Reliability Engineering and System Safety,* **122** (2) 74–95.

[21] R.P. Rechard. 2025. Low probability rationale for excluding post-closure criticality at Waste Isolation Pilot Plant along with risk perspective; Memorandum to Steve Wagner, 8880; Ross Kirkes, 8883; ERMS Albuquerque, NM: Sandia National Laboratories.

[22] R.P. Rechard, B. Reedlunn, J.E. Bean, Jr., B.A. Day, and L.C. Sanchez. 2025. Improbability of post-closure criticality in array of transuranic waste containers after compaction by salt creep at Waste Isolation Pilot Plant, SAND2025. Albuquerque, NM: Sandia National Laboratories.

[23] R.P. Rechard. 2019. Improbability of transuranic waste compaction by salt creep causing criticality in bedded salt repository; Memorandum to Paul E. Shoemaker, 8880; Todd Zeitler, 8863; Ross Kirkes,

Information Only

8883; November 2019, Albuquerque, NM: Sandia National Laboratories.

[24] R.P. Rechard, B.A. Day, B. Reedlunn, and J.E. Bean, Jr. 2025. Improbability of post-closure criticality in compacted criticality control overpacks after room closure at Waste Isolation Pilot Plant, SAND2025. Albuquerque, NM: Sandia National Laboratories.

[25] R.P. Rechard, B.A. Day, B. Reedlunn, and J.E. Bean, Jr. 2022. Improbability of nuclear criticality in criticality control overpacks after salt creep compaction at Waste Isolation Pilot Plant, SAND2022-0952. Albuquerque, NM: Sandia National Laboratories.

[26] R.P. Rechard. 2025. Fissile mass and concentration necessary for post-closure criticality in geologic media near bedded salt repository Memorandum to Steve Wagner, 8880; Ross Kirkes, 8883; October 2025, ERMS. Albuquerque, NM: Sandia National Laboratories.

[27] R.P. Rechard, L.C. Sanchez, P.J. McDaniel, J. Hunt, and G. Broadous, Fissile mass and concentration criteria in geologic media near bedded salt repository presented at the International High-Level Radioactive Waste Management Conference, April 14-18, 2019, Knoxville, TN, 2019.

[28] R.P. Rechard, L.C. Sanchez, M. Olgvun, and G. Ryba. 2019. Fissile mass and concentration necessary for criticality in geologic media near bedded salt repository, Memorandum to Paul E. Shoemaker, 8880; Todd Zeitler, 8862; Ross Kirkes, 8883; November 2019, Albuquerque, NM: Sandia National Laboratory.

[29] EPA (US Environmental Protection Agency). 1996. Compliance application guidance for 40 CFR 194, EPA-402-R-95-014. Washington, DC: Office of Radiation and Indoor Air, US Environmental Protection Agency.

[30] EPA (US Environmental Protection Agency). 2008. 40 CFR Part 197: Public health and environmental radiation protection standards for Yucca Mountain, Nevada; final rule. *Federal Register,* **73** (200) 61256:61289.

[31] R.P. Rechard. 1996. An introduction to the mechanics of performance assessment using examples of calculations done for the Waste Isolation Pilot Plant between 1990 and 1992, SAND93-1378 revised. Albuquerque, NM: Sandia National Laboratories.

[32] R.P. Rechard, W. Beyeler, R.D. McCurley, D.K. Rudeen, J.E. Bean, and J.D. Schreiber. 1990. Parameter sensitivity studies of selected components of the Waste Isolation Pilot Plant repository/shaft system, SAND89-2030. Albuquerque, NM: Sandia National Laboratories.

[33] M.G. Marietta, S.G. Bertram-Howery, D.R. Anderson, K.F. Brinster, R.V. Guzowski, H. Iuzzolino, and R.P. Rechard. 1989. Performance assessment methodology demonstration: Methodology development for evaluating compliance with EPA 40 CFR 191, Subpart B, for the Waste Isolation Pilot Plant, SAND89-2027. Albuquerque, NM: Sandia National Laboratories.

[34] EPA (US Environmental Protection Agency). 1985. Background information document: Final rule for high-level and transuranic radioactive wastes, EPA 520/1-85-023. Washington, DC: US Environmental Protection Agency, Office of Radiation Programs.

[35] DOE (US Department of Energy). 1996. Final programmatic environmental impact statement, EIS-0229. Washington, DC: US Department of Energy.

[36] DOE (US Department of Energy). 2004. Title 40 CFR Part 191: Compliance recertification application for the Waste Isolation Pilot Plant, DOE/WIPP 2004-3231. Carlsbad, NM: Waste Isolation Pilot Plant, Carlsbad Field Office, US Department of Energy.

[37] C.D. Leigh, J. Trone, and B. Fox. 2005. TRU waste inventory for the 2004 compliance recertification application performance assessment baseline calculation, ERMS 541118. Carlsbad, NM: Sandia National Laboratories.

[38] B. Crawford, D. Guerin, S. Lott, W. McInroy, J. McTaggart, and G.D. Van Soest. 2009. Performance assessment inventory report - 2008, INV-PA-08, Revision 0. Carlsbad, NM: Los Alamos National Laboratory, Carlsbad Operations.

[39] D.J. Clayton, S.C. Dunagan, J.W. Garner, A.E. Ismail, T.B. Kirchner, G.R. Kirkes, and M.B. Nemer. 2008. Summary report of the 2009 compliance recertification application performance assessment, ERMS 548862. Carlsbad, NM: Sandia National Laboratories.

[40] G.D. Van Soest. 2018. Performance assessment inventory report - 2018, INV-PA-18, Revision 0. Carlsbad, NM: Los Alamos National Laboratory.

[41] G.D. Van Soest. 2022. Performance assessment inventory report - 2022, INV-PA-22, Revision 0. Carlsbad, NM: Los Alamos National Laboratory.

[42] D.C. Kicker. 2023. Radionuclide inventory screening analysis for the replacement panels planned change request performance assessment (RPPCR PA), ERMS 578878. Carlsbad, NM: Sandia National Laboratories.

[43] D.C. Kicker. 2025. Analysis Report for Radionuclide Inventory Screening in the 2026 Compliance Recertification Application Performance Assessment: Interim State Repository, ERMS. Carlsbad, NM: Sandia National Laboratories.

[44] G.D. Van Soest. 2025. Full repository performance assessment inventory report - 2024, INV-FPA-24. Carlsbad, NM: Los Alamos National Laboratory.

[45] D.C. Kicker. 2025. Analysis Report for Radionuclide Inventory Screening in the 2026 Compliance Recertification Application Performance Assessment: Final State Repository, ERMS Carlsbad, NM: Sandia National Laboratories.

[46] R.J. MacKinnon, G.A. Freeze, and H. Jow. 1997. Summary of EPA-mandated performance assessment verfication test (replicate 1) and cmoparison with the compliance certificatin

Information Only

application calculations, revision 1, ERMS 541521. Carlsbad, NM: Sandia National Laboratories.

[47] D.J. Clayton, R.C. Camphouse, J.W. Garner, A.E. Ismail, T.B. Kirchner, K.L. Kuhlman, and M.B. Nemer. 2010. Summary report of the CRA-2009 performance assessment baseline calculation, ERMS 559466. Carlsbad, NM: Sandia National Laboratories.

[48] H.K. Clark. 1981. Subcritical limits for plutonium systems. *Nuclear Science and Engineering,* **79** (1) 65–84, doi: 10.13182/NSE81-A19043.

[49] ANSI (American National Standards Institute). 2014. An American national standard for nuclear criticality safety in operations with fissionable materials outside reactors, ANSI/ANS-8.1-2014. La Grange Park, IL: American National Standards Institute.

[50] DOE (US Department of Energy). 2024. Response 4 to the US Environmental Portection Agency's question on the Replacment Planels Planned Change Request. Letter to Tom Peake, Director Center for Waste Management and Regulations from Michael Gerl, Director Environmental Regulatory Compliance Division, Carlsbad Field Office, US Department of Energy, ERMS. Carlsbad, NM: US Department of Energy, Carlsbad Field Office.

[51] G.D. Van Soest. 2022. Performance assessment inventory report - 2021 for the replacement panels planned change request, INV-RPA-21, Rev. 0. Carlsbad, NM: Los Alamos National Laboratory.

[52] D.E. Munson, A.F. Fossum, and P.E. Senseny. 1989. Advances in resolution of discrepancies between predicted and measured in situ WIPP room closures, SAND88-2948. Albuquerque, NM: Sandia National Laboratories.

[53] B. Reedlunn and J.E. Bean, Jr. 2021. Additional simulations of criticality control overpack and pipe overpack container compaction at the Waste Isolation Pilot Plant SAND2021-11268 CTF. Albuquerque, NM: Sandia National Laboratories.

[54] M.D. Siegel, S.J. Lambert, and K.L. Robinson. 1991. Hydrogeolchemical studies of the Rustler Formation and related rocks in the Waste Isolation Pilot Plant area, southeastern New Mexico, SAND88-0196. Albuquerque, NM: Sandia National Laboratories.

[55] Accident Investigation Board and DOE (US Department of Energy). 2014. Radiological release event at the Waste Isolation Pilot Plant on February 14, 2014, Accident Investigation Report, Washington, DC: US Department of Energy, Office of Environmental Management. [Online]. Available: https://wipp.energy.gov/wipprecovery-accident-desc.asp

[56] L.H. Brush. 1990. Test plan for laboratory and modeling studies of repository and radionuclide chemistry for the Waste Isolation Pilot Plant, SAND90-0266. Albuquerque, NM Sandia National Laboratories.

[57] L.H. Brush and P.S. Domski. 2014. Prediction of baseline actinide solubilities for the WIPP CRA-2014 PA, AP-153, Rev. 1 records package. Carlsbad, NM: Sandia National Laboratories.

[58] H.W. Papenguth and Y.K. Behl. 1996. Test plan: Evaluation of dissolved actinide retardation at the Waste Isolation Pilot Plant, TP 96-02. WPO 31336. Albuquerque, NM: Sandia National Laboratories.

[59] P.S. Domski. 2025. Prediction of baseline actinide solubilities for the 2026 WIPP Compliance Recertification Performance Assessment final-state analysis (CRA-2026 FS), ERMS. Albuquerque, NM: Sandia National Laboratories.

[60] R.S. Popielak, R.L. Beauheim, S.R. Black, W.E. Coons, C.T. Ellingson, and R.L. Olsen. 1983. Brine reservoirs in the Castile Formation, Waste Isolation Pilot Plant Project, sourtheastern New Mexico, TME 3153. Carlsbad, NM: U.S. Department of Energy, WIPP Project Office.

[61] K.F. Eckerman, A.B. Wolbarst, and C.B. Richardson. 1988. Limiting values of radionuclide intake and air concentration and dose conversion factors for inhalation, submersion, and ingestion, EPA 520/1-88-020. Federal Guidance Report No. 11. Washington, DC: US Environmental Protection Agency.

[62] S.C. Babb and C.F. Novak. 1995. FMT, Version 2.0, User's Manual, WPO 28119. Carlsbad, NM: Sandia National Laboratories.

[63] T.J. Wolery. 1992. EQ3/6, a software package for geochemical modeling of aqueous systems: Overview and installation guide (ver. 7), UCRL-MA-110662. Livermore, CA: Lawrence Livermore National Laboratory.

[64] Y. Xiong. 2011. Release of EQ3/6 database DATA0.FM1. E-mail to Jennifer Long, March 9, 2011, ERMS 555152. Carlsbad, NM: Sandia National Laboratories.

[65] C.T. Stockman, J.W. Garner, J.C. Helton, J.D. Johnson, A. Shinta, and L.N. Smith. 2000. Radionuclide transport in the vicinity of the repository and associated complementary cumulative distribution functions in the 1996 performance assessment for the Waste Isolation Pilot Plant. *Reliability Engineering and Systems Safety,* **69** (1-3) 369–396.

[66] P.V. Brady, H.W. Papenguth, and J.W. Kelly. 1999. Metal sorption to Dolomite surfaces. *Appl. Geochem.,* **14** (5) 569.

[67] D. Langmuir, *Aqueous environmental geochemistry*. Prentice Hall, 1997.

[68] D.J. Clayton. 2008. Update to the calculation of the minimum brine volume for a direct brine release, EMRMS 548522. Albuquerque, NM: Sandia National Laboratories.

[69] S. King. 2021. Repository volume, DRZ volume, and minimum brine volume for a direct brine release for repository with new panels, ERMS 576475. Albuquerque, NM: Sandia National Laboratories.

[70] P. Docherty. 2024. Update to WIPP PA parameter DBRMINBV, ERMS. Carlsbad, NM: Sandia National Laboratories.

Information Only

[71] C. Vignes, J.E. Bean, Jr., and B. Reedlunn. 2023. Improved modeling of Waste Isolation Pilot Plant disposal room porosity, SAND2023-04826. Albuquerque, NM: Sandia National Laboratories.

[72] L.C. Sanchez, P.E. Drez, and J.S. Rath. 2000. Radioactive and nonradioactive waste intended for disposal at the Waste Isolation Pilot Plant. *Reliability Engineering and System Safety,* **69** (1-3) 99–108.

[73] P.E. Drez. 1996. Final preliminary estimate of complexing agents in TRU solidified waste forms scheduled for disposal in WIPP, ERMS 235552. Carlsbad, NM: Sandia National Laboratories.

[74] Y. Wang and L.H. Brush. 1996. Estimates of gas-generation parameters for the long-term WIPP performance assessment, memorandum to M.S. Tierney, January 26, 1996, ERMS 231943. Albuquerque, NM: Sandia National Laboratories.

[75] Y. Wang and L.H. Brush. 1996. Modify the stoichiometric factor y in the BRAGFLO to include the effect of MgO added to WIPP repository as a backfill, memorandum to M.S. Tierney, February 23, 1996, ERMS 232286. Albuquerque, NM: Sandia National Laboratories.

[76] J. Reyes. 2008. Letter to D.C. Moody (5 Enclosures). 11 February 2008., ERMS 549331. Washington, DC: US Environmental Protection Agency, Office of Radiation and Indoor Air.

[77] J.C. Helton, J. Bean, J.E., J.W. Berglund, F.J. Davis, K. Economy, J.W. Garner, J.D. Johnson, R.J. MacKinnon, J. Miller, D.G. O`Brien, J.L.J. Ramsey, J.D. Schreiber, A. Shinta, L.N. Smith, D.M. Stoelzel, C.T. Stockman, and P. Vaughn. 1998. Uncertainty and sensitivity analysis results obtained in the 1996 performance assessment for the Waste Isolation Pilot Plant, SAND98-0365. Albuquerque, NM: Sandia National Laboratories.

[78] P.S. Domski. 2025. Uncertainty analysis of actinide solubiliities for the2026 Compliance Recertification Application (CRA-2026), ERMS. Albuquerque, NM: Sandia National Laboratories.

[79] Y. Xiong and P.S. Domski. 2016. Uncertainty analysis of actinide solubilities for CRA 2014 sensitivity investigation number 4, ERMS 567306. Carlsbad, NM: Sandia National Laboritories.

[80] H.W. Papenguth and R.C. Moore. 1996. Attachement A: Rationale for definition of parameter values for mineral fragment type colloids, WPO 35855. Albuquerque, NM: Sandia National Laboratories.

[81] H.W. Papenguth. 1996. Attachment A: Rationale for definition of parameter values for actinide intrinsic colloids, WPO 35852. Albuquerque, NM: Sandia National Laboratories.

[82] H.W. Papenguth and R.C. Moore. 1996. Attachment A: Rationale for definition of parameter values for humic substances, WPO 35855. Albuquerque, NM: Sandia National Laboratories

[83] H.W. Papenguth. 1996. Attachment A: Rationale for definition of parameter values for microbes, WPO 35856. Albuquerque, NM: Sandia National Laboratories.

[84] ATSDR (Toxic Substances and Disease Registry). Toxicological profile for plutonium [Online] Available: https://www.atsdr.cdc.gov/ToxProfiles/tp143.pdf

[85] ATSDR (Toxic Substances and Disease Registry). Toxicological profile for americium [Online] Available: https://atsdr.cdc.gov/ToxProfiles/tp156.pdf

[86] ATSDR (Toxic Substances and Disease Registry). Toxicological profile for thorium [Online] Available: https://atsdr.cdc.gov/ToxProfiles/tp147.pdf

[87] N. Morelova. 2020. Steel corrosion and actinide sorptin by iron corrosion products under saline conditions, PhD dissertation. Karlsruher INstintue fur Technologie (KIT).

[88] P. Lin, M. Chen, and L. Guo. 2015. Effect of naural organic matter on the adsorption and fractionation of thorium andprotactinium on nanoparticles in seawater. *Marine Chemistry,* **173** 291–301.

[89] A.A. Christy. 2008. Quantitative determination of surface area of silica gel particles by near infrared spectroscopy and chemometrics. *Colloids and Surfaces: Physicochemical and Engineering Aspects* **322** (1-3) 248–252.

[90] E. Bohnert, C. Borkel, B. Kienzler, V. Metz, N. Finck, T. Rabung, M. Schlieker, and M. Wiedemann. 2018. Chapter 5.2 Non-heat produing waste forms and barrier materials, Annual Report 2015; https://core.ac.uk/download/pdf/197532395.pdf#page=39. Institute for Nuclear Waste Disposal/KIT Institut fur Nukleare Entsorgung.

[91] J.D. Farr, R.K. Schulze, and B.D. Honeyman. 2000. Aqueous Pu (IV) sorption on brucite. *Radiochimica Acta,* **88** (9-11) 675–680.

[92] R.M. Holt. 1997. Conceptual model for transport processes in the Culebra Dolomite Member, Rustler Formation, SAND97-0194. Albuquerque, NM: Sandia National Laboratories.

[93] Y. Cudennec and A. Lecerf. 2006. The transformation of ferrihydrite into goethite or hematite, revisited. *Journal of Solid State Chemistry,* **179** 716–722.

[94] C. Liu, Z. Zhu, F. Li, T. Liu, C. Liao, J.-J. Lee, K. Shih, L. Tao, and Y. Wu. 2016. Fe(II)-induced phase transormation of ferrihydrite: the inhibition effects and stabilization of divalent metal cations. *Chemical Geology,* **444** 110–119.

[95] Z. Wang, R.C. Moore, M.J. Mason, and R.K. Kukkadapu. 2001. A study of corrosion products of mild steel in high ionic strength brines. *Waste Management,* **21** (4) 335–341.

[96] C. Hansel, M., S.G. Benner, and S. Fendorf. 2005. Competing Fe(II)-induced mineralization pathways of Ferrihydrite. *Envionmental Science Technology,* **39** (18) 7147–7153.

Information Only

[97] J.A. Davis and D.B. Kent, Surface complexation modeling in aqueous geochemistry, in *Mineral-Water Interface Geochemistry, M.F. Hochella, Jr., and A.F. White (Eds.)*, vol. 23, (Reviews in Mineralogy, no. 177): Mineralogical Society of America, 1990.

[98] T.R. Zeitler, B.A. Day, J. Bethune, R. Sarathi, and J. Long. 2017. Assessment of abandoned panel closures in south end of repository and lack of waste emplacement in panel 9, ERMS 568459. Carlsbad, NM: Sandia National Laboratories.

[99] K.G. Bell. 1963. Uranium in carbonate rocks, Professional Paper 474-A. US Geological Survey.

[100] R. Sarathi. 2019. Analysis package for actinide mobilization and Salado transport in the 2019 compliance recertification application performance assessment (CRA-2019 PA), ERMS 571371. Carlsbad, NM: Sandia National Laboratories.

[101] B.A. Day. 2019. Analysis package for Salado flow in the 2019 compliance recertification application performance asssessment (CRA 2019 PA), ERMS 571368. Carlsbad, NM: Sandia National Laboratories.

[102] P.N. Swift and T.F. Corbet. 2000. The geologic and hydrogeologic setting of the Waste Isolation Pilot Plant. *Reliability Engineering and System Safety,* **69** (1-3) 47–58.

[103] T. Corbet. 1996. Expedited CCA activity: geochemistry/hydrology issue in Culebra, WPO 42315. Albuquerque, NM: Sandia National Laboratories.

[104] G.E. Hammond, P.C. Lichtner, and R.T. Mills. 2014. Evaluating the performance of parallel subsurface simulators: an illustrative example with PFLOTRAN. *Water Resources Research,* **50**, doi: 10.1002/2012WR013483.

[105] M. Feng and T. LaForce. 2019. Qualification test for PFLOTRAN, ERMS 572028 in WIPP Central File. Carlsbad, NM: Sandia National Laboratories.

[106] K. Kuhlman. 2010. Analysis report for the CRA-2009 PABC Culebra flow and transport calculations, AP-144, ERMS 552951. Carlsbad, NM: Sandia National Laboratories.

Information Only

Information Only